

2015-07-01

New insights into landslide processes around volcanic islands from Remotely Operated Vehicle (ROV) observations offshore Montserrat

Watt, SFL

<http://hdl.handle.net/10026.1/12144>

10.1002/2015GC005781

Geochemistry, Geophysics, Geosystems

All content in PEARL is protected by copyright law. Author manuscripts are made available in accordance with publisher policies. Please cite only the published version using the details provided on the item record or document. In the absence of an open licence (e.g. Creative Commons), permissions for further reuse of content should be sought from the publisher or author.



RESEARCH ARTICLE

10.1002/2015GC005781

Key Points:

- Novel ROV data enhance understanding of submarine volcanic landslide emplacement
- Substrate interaction and distinct morphologies among differences from subaerial equivalents
- Offshore record augments onshore data and indicates diversity of landslide processes around islands

Supporting Information:

- Supporting Information S1
- Movie S1
- Movie S2
- Movie S3
- Movie S4
- Movie S5
- Movie S6
- Movie S7
- Movie S8
- Movie S9
- Movie S10

Correspondence to:

S. F. L. Watt,
s.watt@bham.ac.uk

Citation:

Watt, S. F. L., et al. (2015), New insights into landslide processes around volcanic islands from Remotely Operated Vehicle (ROV) observations offshore Montserrat, *Geochem. Geophys. Geosyst.*, 16, 2240–2261, doi:10.1002/2015GC005781.

Received 19 FEB 2015

Accepted 7 JUN 2015

Accepted article online 11 JUN 2015

Published online 14 JUL 2015

New insights into landslide processes around volcanic islands from Remotely Operated Vehicle (ROV) observations offshore Montserrat

S. F. L. Watt¹, M. Jutzeler², P. J. Talling², S. N. Carey³, R. S. J. Sparks⁴, M. Tucker⁴, A. J. Stinton⁵, J. K. Fisher⁶, D. Wall-Palmer⁶, V. Hühnerbach², and S. G. Moreton⁷
¹School of Geography, Earth and Environmental Sciences, University of Birmingham, Birmingham, UK, ²National Oceanography Centre, Southampton, UK, ³Graduate School of Oceanography, University of Rhode Island, Kingston, Rhode Island, USA, ⁴School of Earth Sciences, University of Bristol, Bristol, UK, ⁵Montserrat Volcano Observatory, Flemmings, Montserrat, West Indies, ⁶School of Geography, Earth and Environmental Sciences, Plymouth University, Plymouth, UK, ⁷NERC Radiocarbon Facility (East Kilbride), Scottish Enterprise Technology Park, East Kilbride, UK

Abstract Submarine landslide deposits have been mapped around many volcanic islands, but interpretations of their structure, composition, and emplacement are hindered by the challenges of investigating deposits directly. Here we report on detailed observations of four landslide deposits around Montserrat collected by Remotely Operated Vehicles, integrating direct imagery and sampling with sediment core and geophysical data. These complementary approaches enable a more comprehensive view of large-scale mass-wasting processes around island-arc volcanoes than has been achievable previously. The most recent landslide occurred at 11.5–14 ka (Deposit 1; 1.7 km³) and formed a radially spreading hummocky deposit that is morphologically similar to many subaerial debris-avalanche deposits. Hummocks comprise angular lava and hydrothermally altered fragments, implying a deep-seated, central subaerial collapse, inferred to have removed a major proportion of lavas from an eruptive period that now has little representation in the subaerial volcanic record. A larger landslide (Deposit 2; 10 km³) occurred at ~130 ka and transported intact fragments of the volcanic edifice, up to 900 m across and over 100 m high. These fragments were rafted within the landslide, and are best exposed near the margins of the deposit. The largest block preserves a primary stratigraphy of subaerial volcanic breccias, of which the lower parts are encased in hemipelagic mud eroded from the seafloor. Landslide deposits south of Montserrat (Deposits 3 and 5) indicate the wide variety of debris-avalanche source lithologies around volcanic islands. Deposit 5 originated on the shallow submerged shelf, rather than the terrestrial volcanic edifice, and is dominated by carbonate debris.

1. Introduction

Extensive submarine landslide deposits are common around volcanic islands [Moore *et al.*, 1989; Deplus *et al.*, 2001; Masson *et al.*, 2002; Coombs *et al.*, 2007; Silver *et al.*, 2009]. Such landslides profoundly modify island morphology and affect the marine environment through sudden deposition of material. They also pose major hazards through direct inundation [Siebert, 1984], their potential association with explosive volcanic blasts [Bogoyavlenskaya *et al.*, 1985], and tsunamis [Ward and Day, 2003; Satake, 2007]. Much of our current understanding of large landslide deposits around volcanic islands is based on geophysical surveys [e.g., Deplus *et al.*, 2001; Coombs *et al.*, 2007; Watt *et al.*, 2012a] and distal core samples of associated turbidites [Hunt *et al.*, 2011; Trofimovs *et al.*, 2013]. Only a few submarine volcanic landslide deposits have been observed or sampled directly [Yokose, 2002; Morgan *et al.*, 2007; Croff Bell *et al.*, 2013; Day *et al.*, 2015]. Such observations provide structural and lithological information relating to the landslide source and emplacement processes that cannot be obtained by other means.

In this paper, we summarize results from two Remotely Operated Vehicle (ROV) surveys of four landslide deposits offshore the volcanic island of Montserrat. Our aim is to provide detailed information on the source (e.g., subaerial edifice, submarine flank, surrounding seafloor), lithology (e.g., pyroclastic rock, dense lava, carbonate reef), and structure (e.g., heterogeneous, disaggregated material; intact primary blocks) of material within the deposits. This informs our understanding of the relationship between the dominant lithology and morphology of landslide deposits [cf. Masson *et al.*, 2006] and helps interpret landslide emplacement processes and interaction with the seafloor, which is a significant control on the magnitude of landslide-generated tsunamis [Watt *et al.*, 2012a].

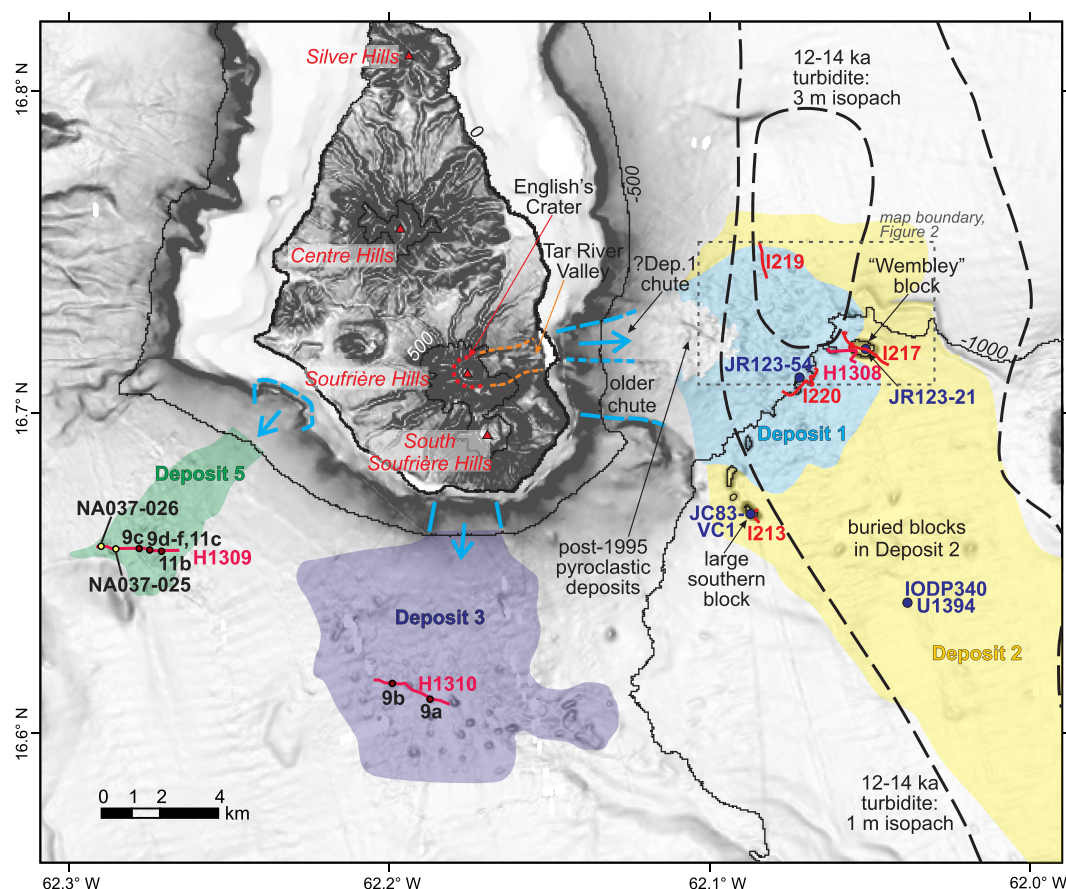


Figure 1. Topographic and bathymetric map of Montserrat, showing the offshore debris-avalanche deposits 1, 2, 3, and 5 [Lebas *et al.*, 2011; Watt *et al.*, 2012b]. Deposits 1, 3, and 5 are well exposed near the seafloor, while Deposit 2 is partially buried but evident from the bathymetric expression of individual large blocks. Dive sites discussed in the text are marked: Isis dives, from cruise JC83, are prefixed I; Hercules dives, from cruise NA037, are prefixed H. Selected vibracore locations, collected on cruise JCR123 [Trofimovs *et al.*, 2008, 2010], are also marked. Points prefixed NA037 show the location of samples discussed in the text, and numbered points refer to images in subsequent figures. Isopachs for the 12–14 ka turbidite are taken from Trofimovs *et al.* [2010].

1.1. Data Collection

Two research expeditions of the RRS *James Cook* (JC83; March 2013) and the R/V *Nautilus* (NA037; October 2013) deployed Remotely Operated Vehicles (ROVs) offshore Montserrat to investigate submarine landslide deposits through high-definition video filming, still images, and a remotely manipulated sampling arm. Expedition JC83 deployed the Isis ROV, collecting footage during four dives SE of Montserrat (Figure 1; Isis dive numbers are prefixed I). Dimensions of outcrops and rocks were estimated using two laser points in the ROV field of view, which are 10 cm apart. A vibrocore attachment collected a single core during Dive I213, but this attachment, as well as the manipulator arm, was not operational during the remainder of the cruise. Expedition NA037 [Carey *et al.*, 2014] deployed a two-vehicle ROV system (Hercules and Argus) during three dives south and east of Montserrat. In addition to imagery, it collected 61 samples via a manipulator arm (Figure 1; Hercules/Argus dive numbers are prefixed H). The largest rocks or consolidated-sediment samples that could be collected were 20 cm in diameter.

ROV-based technology has been used in Hawaii to investigate submarine volcanic-island landslide processes [Yokose, 2002; Coombs *et al.*, 2004; Yokose and Lipman, 2004; Morgan *et al.*, 2007], but our work is among the first to apply such methods elsewhere [cf. Croff Bell *et al.*, 2013].

1.2. Terminology

Following past studies around volcanic islands [e.g., Moore *et al.*, 1989; Masson *et al.*, 2002], we use *landslide* as a general term for any slope failure and the resulting mass movement. The landslide deposits described here originated as failures of rock on the subaerial and submerged island flanks, which fragmented to form

a *debris avalanche*, where the disintegrating mass is dispersed between clearly defined source and depositional regions. Progressive fragmentation and spreading results in the characteristic hummocky topography of debris-avalanche deposits [Siebert, 1984; Glicken, 1996; Paguican *et al.*, 2014], but the specific character of the debris avalanche (and its deposit) may depend on the nature of material within the landslide (e.g., density, strength, homogeneity) [Naranjo and Francis, 1987; Masson *et al.*, 2006; Dufresne and Davies, 2009; Watt *et al.*, 2014]. Debris avalanches originating in clay-rich terrains, such as hydrothermally altered portions of volcanic edifices, may be relatively cohesive. The incorporation of basal sediment (e.g., hemipelagic mud from the seafloor) may also promote more cohesive flow characteristics. For simplicity, we use *debris-avalanche deposit* to refer to all deposits, rich in volcanic rock fragments, that directly result from the initial landslide. In marine environments, seafloor-sediment failure [Watt *et al.*, 2012b, 2014] associated with debris-avalanche emplacement may produce more extensive deposits. In addition, landslides around volcanic islands may generate dilute and highly mobile *turbidity currents* [Talling *et al.*, 2012] from the mixing of primary landslide material or disrupted marine sediment with seawater, depositing *turbidites*.

2. Study Region

Montserrat is located in the northern Lesser Antilles Arc and comprises four volcanic centers dating back to at least 2.5 Ma (Figure 1) [Harford *et al.*, 2002]. The andesitic Soufrière Hills volcano has been active since 250 ka [Harford *et al.*, 2002; Smith *et al.*, 2007], interrupted by a short episode of basaltic volcanism at ~130 ka that formed the South Soufrière Hills center. An important aspect of the geological history of Soufrière Hills (and of Montserrat in general) is the occurrence of large landslides. Several debris-avalanche deposits, with volumes between 0.3 and 10 km³, have been identified offshore southern Montserrat from geophysical surveys [Le Friant *et al.*, 2004; Lebas *et al.*, 2011; Watt *et al.*, 2012a, 2012b]. In addition to these surveys, the identification and correlation of tephra fall deposits and turbidites within marine sediment cores provides a detailed record of past activity on the island [Le Friant *et al.*, 2009, 2015; Trofimovs *et al.*, 2013; Cassidy *et al.*, 2013; Wall-Palmer *et al.*, 2014]. These studies provide age constraints on landslide deposits and contribute to understanding the context of major landslides in the broader volcanic history of the island. However, direct core sampling of the block-rich volcanic landslide deposits has been unsuccessful, because of their coarse and heterogeneous nature.

The 1995-to-recent eruption of Soufrière Hills has involved the growth and collapse of a series of andesitic lava domes, generating pyroclastic flows [Wadge *et al.*, 2014]. The largest dome collapse, in 2003, involved >0.21 km³ of material [Herd *et al.*, 2005]. East of Montserrat, submarine deposits from several collapse-driven pyroclastic flows have formed lobes with a cumulative thickness of 100 m, extending 7 km from the coastline (Figure 1) [Trofimovs *et al.*, 2008; Le Friant *et al.*, 2009].

2.1. Terrestrial Morphology and Landslide Scars

Prior to its recent activity, Soufrière Hills consisted of a series of lava domes surrounding a prominent crescent-shaped collapse scar (English's Crater). This scar was open to the east and led directly into the Tar River valley (Figure 1). English's Crater has been the location of lava extrusion since 1995, and is presently occupied by a lava dome with a volume of >0.19 km³ [Stinton *et al.*, 2014]. Dating of material within English's Crater shows that two eruptive or mass-wasting events, of unconstrained size, occurred at ~2 and ~6 ka [Smith *et al.*, 2007; Boudon *et al.*, 2007]. This indicates that the crater formed at ≥6 ka.

East of the Tar River valley, a 3.5 km wide chute is cut into the submerged SE flank of Montserrat (Figure 1) [Le Friant *et al.*, 2004]. This chute is attributed to a large landslide that formed an elongate offshore deposit named Deposit 2 [Le Friant *et al.*, 2004]. Within the northern part of the chute, a 1.2 km wide depression aligns closely with the Tar River valley and English's Crater. Collectively, these structures may mark the source and pathway of an offshore landslide deposit named Deposit 1 [Le Friant *et al.*, 2004; Lebas *et al.*, 2011]. Deposit 1 has a volume of 1.7 km³, while English's Crater represents ~0.5 km³ of missing rock [Le Friant *et al.*, 2004]. The submerged chute has a volume of ~0.5 to 1.1 km³ [Watt *et al.*, 2012b] but may be partly infilled by later aggradation. Notwithstanding the large uncertainties (owing, e.g., to a lack of constraints on preexisting topography), these estimated volumes suggest that Deposit 1 comprises both subaerial material from English's Crater and submerged material from the northern part of the chute. A reduced bulk density and seafloor-sediment incorporation may account for some increase in the deposit volume versus the inferred failure volume.

Two further landslide deposits, termed Deposits 3 and 5, are located south of Montserrat (Figure 1; note that Deposit 4 is buried beneath Deposit 3 and is not discussed further here). These deposits align with scars in the island shelf but are not associated with any visible subaerial collapse structures.

2.2. Morphological Description of Landslide Deposits

Deposits 1, 2, 3, and 5 are all defined by mounded, irregular areas of seafloor (Figure 1). Within each deposit, the mounded surface may either represent hummocks—hills of amalgamated landslide material, typical of subaerial debris-avalanche deposits [Siebert, 1984]—or individual scattered blocks, representing largely intact fragments of the initial landslide mass [cf. Watt *et al.*, 2014].

2.2.1. Deposit 1

The margin of Deposit 1 is defined as the limit of a hummocky, fan-shaped deposit that extends 10.5 km offshore the Tar River valley, to water depths of 1000 m, and covers $\sim 50 \text{ km}^2$. The deposit contains many tens of hummocks that are up to 200 m long and protrude tens of meters above surrounding seafloor. The hummocks are evenly distributed, without preferential accumulation at the margins or center of the deposit. Seismic reflection data resolve no prominent internal structures within Deposit 1 [Crutchley *et al.*, 2013; Karstens *et al.*, 2013].

2.2.2. Deposit 2

Deposit 2 is partially buried beneath Deposit 1 and is more extensive and voluminous than the other deposits considered here, comprising $\sim 10 \text{ km}^3$ of material [Lebas *et al.*, 2011; Watt *et al.*, 2012a, 2012b]. It has been proposed that the central, blocky part of Deposit 2 originated as a collapse of the volcanic edifice, which then triggered extensive failure of the surrounding seafloor sediment [Watt *et al.*, 2012b, 2014]. IODP drilling (Figure 1) confirms that the distal part of Deposit 2 comprises seafloor sediment [Le Friant *et al.*, 2015].

Here we attribute the notably large blocks to the east of Montserrat to Deposit 2 (Figure 1), based on interpretations of available seismic and bathymetric data [Watt *et al.*, 2012b]. The most prominent of these blocks lies close to the eastern margin of Deposit 1, and has an angular, steep-sided form that contrasts with the rounded hummocks of Deposit 1. It is 900 m long, 700 m wide, and 100 m high, and may have a similar buried extent, indicating a total volume of $\sim 0.05\text{--}0.08 \text{ km}^3$ [Crutchley *et al.*, 2013]. To place this volume into context, it is approximately 10 times that of Wembley Stadium in London (0.004 km^3), one of the world's largest sports grounds. A 2 km arc of blocks with comparable dimensions to the "Wembley" block (as it is referred to here) marks the proximal southern margin of Deposit 2 (Figure 1). More very large blocks or hummocks occur further east, within the central part of Deposit 2, but are partially buried by younger sediment.

2.2.3. Deposit 3

Deposit 3 extends 10.5 km to the south of Montserrat, reaching water depths of 950 m. Seismic reflection profiles suggest that it is thinner than Deposit 1, and mainly comprises scattered large blocks [Lebas *et al.*, 2011; Watt *et al.*, 2012b] with a total volume of $< 1 \text{ km}^3$.

2.2.4. Deposit 5

Deposit 5 has a poorly constrained volume of $\sim 0.3 \text{ km}^3$ [Le Friant *et al.*, 2004] and is associated with a scar on the submerged coastal shelf on the south-western side of Montserrat. It is defined by a hummocky field of debris that can be traced 7 km offshore to a water depth of about 830 m.

2.3. Ages of Landslide Deposits

Dating of submarine landslide deposits is best achieved by constraining the age and accumulation rate of hemipelagic sediment both above and below the deposit. However, given the difficulties of coring through landslide deposits, ages are often based either on the oldest sediment overlying the deposits or on the age of turbidites that have been correlated with them. In the former approach, the distance between the base of a sediment core and the top of the landslide deposit may be unknown, and any age thus derived is a minimum. In the latter approach, it is potentially difficult to correlate a specific turbidite with a landslide deposit, given that neither necessarily has a unique composition in terms of chemistry or componentry.

2.3.1. Deposit 1

The best direct age constraint for Deposit 1 comes from core JR123-54 (collected in 2005; Figures 1 and 2) [Trofimovs *et al.*, 2013], located on a hummock. The basal unit in the core is a mixed bioclastic and

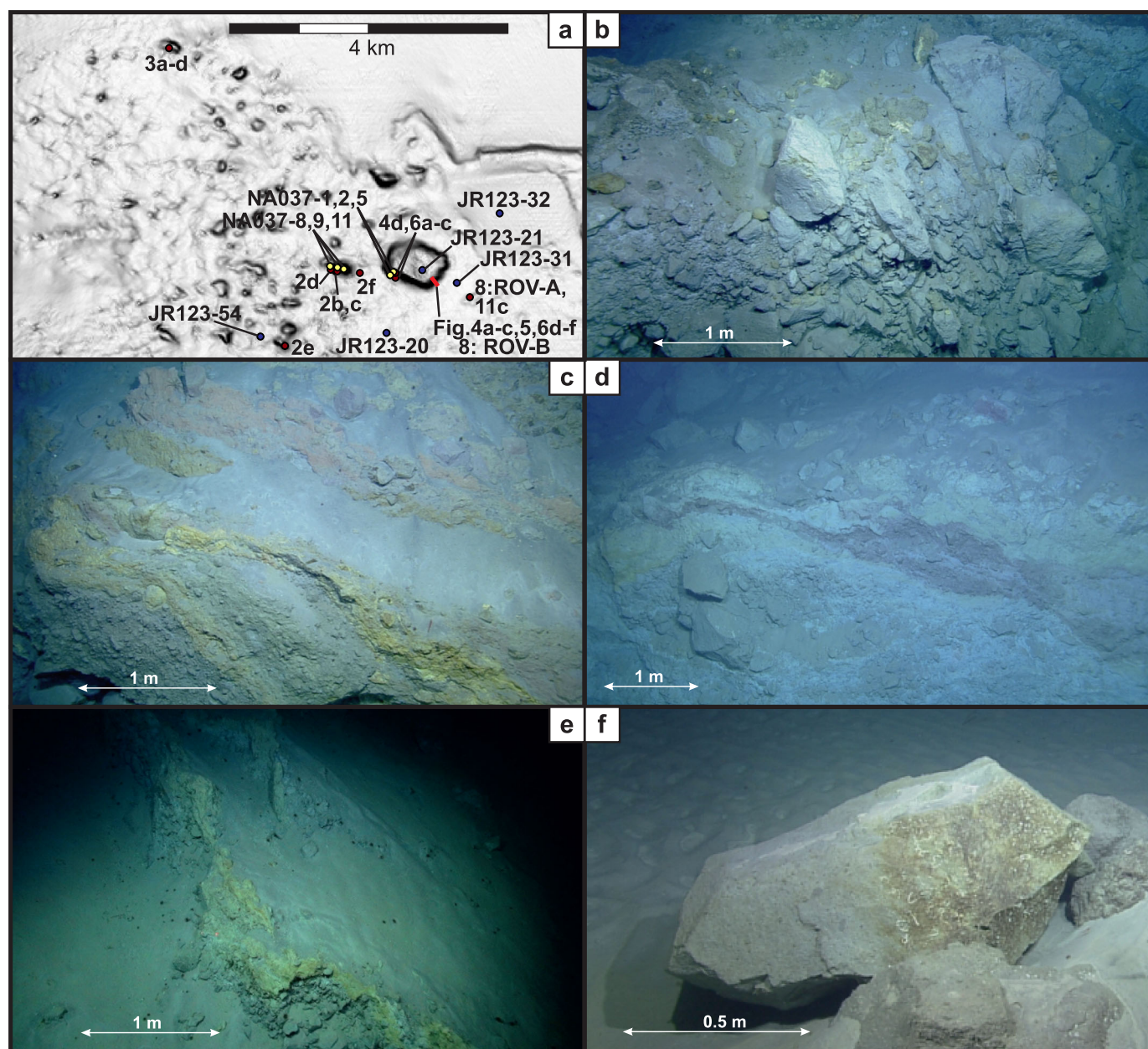


Figure 2. ROV images from hummocks within Deposit 1. (a) Map of image locations (see Figure 1) in this and subsequent figures. Core locations have the prefix JR123, while NA037 marks sample locations referred to in the text. (b) A dense, shattered lava block in contact with yellow, hydrothermally altered material and fresh lava breccia along convolute margins. (c) Dense lava breccias in contact with hydrothermally altered red and yellow deformed domains. (d) Sheared and stretched deformation within hydrothermally altered domains. (e) Vein-like hydrothermal alteration cutting across clast-supported dense lava breccias. (f) Lava block with clear division between fresh and colonized surfaces, potentially indicating a submarine origin for some material mobilized in the Deposit 1 landslide. Figures 2b–2d and 2f are from dive H1308 and Figure 2e from I219.

volcaniclastic turbidite, the lowest part of which comprises poorly sorted gravel containing altered lava clasts, which may correspond to the top surface of Deposit 1 [Trofimovs *et al.*, 2013]. Multiple radiocarbon dates (Table 1) indicate an age of ~ 11.5 ka for this turbidite (a potentially bioturbated sample within the uppermost part of the turbidite provides a maximum age of 12.3 ka).

Deposit 1 may correlate with a large (>0.4 km³) turbidite that extends over 30 km to the south of Montserrat (Figure 1), dated by multiple radiocarbon ages at 12–14 ka [Trofimovs *et al.*, 2013]. The turbidite is by far the largest-volume and most erosive event in the offshore stratigraphy during the past 110 ka, and its thickest part coincides with the margin of Deposit 1. The timing, distribution, and magnitude of the two deposits thus support their correlation. The stratigraphy of the turbidite is complex and

Table 1. Radiocarbon Ages of Monospecific Planktonic Foraminifera (*Globigerinoides ruber*) Picked From Hemipelagic Mud in Core Samples Constraining the Ages of Deposits 1 and 2

Sample name	Publication Code	Depth below Core Top (cm)	Conventional Age (yr BP) (1 σ Error)	Calibrated Age Range ^a (cal yr BP)	$\delta^{13}\text{C}_{\text{VPDB}}\text{‰} \pm 0.1$
JC83-VC1-10 ^b	52752	10–11	1340 (37)	964–781	1.2
JC83-VC1-31 ^b	52753	31–32	3857 (37)	3930–3689	1.6
JC83-VC1-44 ^b	52754	44–45	5615 (37)	6135–5906	1.3
JR123-21-C10	402765	10–11	1870 (30)	1510–1331	0.5
JR123-21-C25	402766	25–26	4760 (30)	5188–4870	1.4
JR123-21-C39	402767	39–40	7450 (30)	7978–7833	1.2
JR123-21-C62	393246	62–65	38940 (400)	43,139–42,035	0.8
JR123-21-C84	402768	84–85	>43,500	NA	0.4
JR123-21-B10	402769	99.5–100.5	>43,500	NA	0.1
JR123-21-B22	393247	112–113	30,280 (150)	34,266–33,692	0.6
JR123-21-B71	402770	160.5–161.5	39,150 (410)	43,311–42,141	0.4
JR123-21-B76	402771	166.5	38,390 (380)	42,763–41,710	0.5
JR123-21-B83	393248	173–174	39,180 (320)	43,191–42,263	0.3
JR123-54 ^{b,c}	12994	235	6802 (35)	7406–7294	0.9
JR123-54 ^{b,c}	12995	242	6330 (35)	6895–6685	0.9
JR123-54 ^{b,c}	23055	273	8794 (37)	9525–9395	1.0
JR123-54 ^c	333973	280	8700 (40)	9465–9269	0.1
JR123-54 ^c	333974	284	8600 (40)	9391–9121	1.7
JR123-54 ^c	333975	294.5	9350 (40)	10,272–10,109	4.4
JR123-54 ^c	333976	303	10830 (50)	12,534–12,085	1.1

^aCalibrated using OxCal4.2 [Bronk Ramsey, 2009] and the Marine13 calibration curve [Reimer et al., 2013]. Calibrated ranges reported at the 95.4% confidence interval. BP refers to years before 1950 A.D.

^bAnalyzed at the NERC Radiocarbon Facility in East Kilbride, UK, following the procedure described in Trofimovs et al. [2013]. Publication codes are SUERC—followed by the listed number; all other samples analyzed at Beta Analytic Inc. Laboratories, Miami.

^cAges previously published in Trofimovs et al. [2013].

spatially variable [Trofimovs et al., 2010], but taken as a whole it comprises equal proportions of biological (calcium carbonate) and volcanic clasts. This contrasts with turbidites derived from pyroclastic flows in the present eruption of Soufrière Hills, which are >95% volcanoclastic [Trofimovs et al., 2008]. Thus, the source event of the 12–14 ka turbidite must have mobilized a significant proportion of submarine, carbonate-rich material, either by contemporaneous failure and disaggregation of carbonate-rich lithologies (i.e., from the island's carbonate shelf), or by erosion of carbonate-rich seafloor sediment. Combining the age determinations from JR123-54 and the mixed turbidite, Deposit 1 occurred at 11.5–14 ka.

2.3.2. Deposit 2

Sediment cores from IODP Expedition 340 (Figure 1) [Le Friant et al., 2015] place the top of Deposit 2 at ~130 ka [Cassidy et al., 2015], based both on oxygen isotope stratigraphy of younger hemipelagic mud and on the correlation of basaltic deposits, which immediately overlie Deposit 2, with volcanism at South Soufrière Hills (dated at 130 ka by Ar-Ar ages of subaerial lavas [Harford et al., 2002]). This age is consistent with an earlier estimate of ~140 ka derived from regional sediment accumulation rates [Watt et al., 2012b].

2.3.3. Deposit 3

A spatial correlation with a mafic volcanoclastic turbidite [Cassidy et al., 2014], dated at 60–130 ka, provides a possible age constraint for Deposit 3. If correct, the correlation implies a mafic source lithology for the landslide. Seismic reflection profiles indicate a sedimentary cover of 5–10 m over Deposit 3, implying an age of 100–200 ka (based on local sedimentation rates of 0.05 m kyr⁻¹ [Watt et al., 2012b]).

2.3.4. Deposit 5

The thickest part of a mixed volcanoclastic and bioclastic turbidite is colocated with Deposit 5, suggesting a correlation between the two deposits [Cassidy et al., 2013]. The high bioclastic content of the turbidite is consistent with the identified landslide source scar on the submerged coastal shelf. The turbidite has an erosive base in hemipelagic sediment dated at 35 ka, and lies directly beneath a volcanoclastic turbidite dated at 8–12 ka. Deposit 5 is therefore similar in age to Deposit 1. The cluster of landslide and turbidite deposits at 8–14 ka suggests a period of relatively heightened mass-wasting activity at Montserrat.

3. New ROV-Based Observations

The principal ROV observations for each landslide deposit are described and interpreted in this section. This interpretation draws on data from preexisting core samples and geophysical data. More specific discussion of landslide processes relating to Deposits 1 and 2 is provided in section 4. In addition to the figures described here, short video files of key exposures are provided as supporting information.

3.1. Deposit 1

3.1.1. Hummock Exposures

ROV observations made on seven hummocks in Deposit 1 (Figure 1) indicate broadly similar mixtures of lithologies, with representative images shown in Figure 2. The top of individual hummocks provides the best outcrops; a talus of scattered rocks and partially eroded sedimentary drape obscure surrounding slopes. Outcrops expose volcanic breccia, with wide variation in grain size, sorting, presence or absence of a fine matrix, presence or absence of layering, clast shape, and alteration. Lithologically diverse domains occur at a range of scales, both within and between hummocks.

A poorly sorted and matrix-supported breccia is the dominant lithology, displaying a range of colorations and with generally sharp, but occasionally diffuse, irregular boundaries between colored domains. Pale colored domains are interpreted as hydrothermally altered volcanic breccias; the diverse coloration (white and pale-yellow are the most common, but green, yellow, orange, and brown also occur) indicates a range of mineral assemblages, and suggests that different zones of hypogene alteration in the failure region [cf. *John et al.*, 2008] were efficiently mixed during debris-avalanche emplacement. Undulose boundaries (Figures 2c and 2d) indicate shearing and stretching of altered domains during transport.

Altered breccias often lie in direct contact with dark gray, monomict, clast-supported to marginally matrix-supported breccias. Clasts are angular to subangular and vary in size from a few meters to a centimeter (Figure 2b). This lithology is interpreted as unaltered autoclastic breccia associated with lava-dome extrusion. Pink to red lava breccias also occur, with otherwise similar characteristics to the monomict gray breccias, and are indicative of hematite formed in a subaerial setting. In one case (Figure 2e), narrow (10–30 cm) and irregular zones of alteration were observed passing through a large outcrop of gray lava breccias.

Samples of the dense lavas (NA037-008 and NA037-011; see supporting information) show a phenocryst assemblage dominated by plagioclase and orthopyroxene, with frequent amphibole largely replaced by an alteration assemblage. This assemblage is typical of Soufrière Hills andesites erupted since ~110 ka [*Harford et al.*, 2002]. We identified no unequivocal biological (carbonate) material or structures within Deposit 1. A sample of orange-brown hydrothermally altered rock (NA037-009; Figure 2a) contained abundant clay minerals and hydrothermally altered ferromagnesian and feldspar crystals.

3.1.2. Deposit 1 Sedimentary Drape

The sedimentary drape that overlies Deposit 1 is well exposed on the sides of several hummocks, where it has been eroded by bottom currents or local slope failures (Figure 3). Interpretations of these exposures have drawn on the extensive previous core sampling of the top ~5 m of seafloor sediment in the area, which comprises an interbedded sequence of hemipelagic mud and volcanoclastic, bioclastic or mixed turbidites (JR123) [*Trofimovs et al.*, 2010, 2013].

The observed exposures comprise a mixture of fine-grained, white to pale-gray hemipelagic sediment and interbedded sandy turbidites. Hemipelagic mud intervals frequently contain coarse volcanic clasts (Figure 3), which are likely to be locally derived (e.g., by reworking from upslope on a hummock). These poorly sorted beds of outsized volcanic clasts set in hemipelagic mud are similar to the talus deposits at the base of the SW Wembley-block exposures (section 3.2.1 and Figure 4d). Bed dips are parallel to the local slope, and sometimes up to 40° (Figure 3b). These heterogeneous beds were not sampled by the JR123 cores, but we note that some attempts at coring failed, perhaps due to the coarse nature of this material.

In several exposures, the basal unit of the drape (i.e., the deposit immediately overlying Deposit 1) is a well-sorted, monomict and clast-supported, matrix-free volcanic breccia of dense, gray centimeter-scale andesite clasts. This unit appears to be relatively continuous over Deposit 1 (Figure 3e). This immature, matrix-free breccia is similar to beds found within volcanic blast deposits on the surface of some subaerial debris-avalanche deposits [*Hoblitt et al.*, 1981; *Bogoyavlenskaya et al.*, 1985; *Clavero et al.*, 2004; *Belousov et al.*, 2007], and provides possible evidence of a lateral explosion accompanying the Deposit 1 landslide.

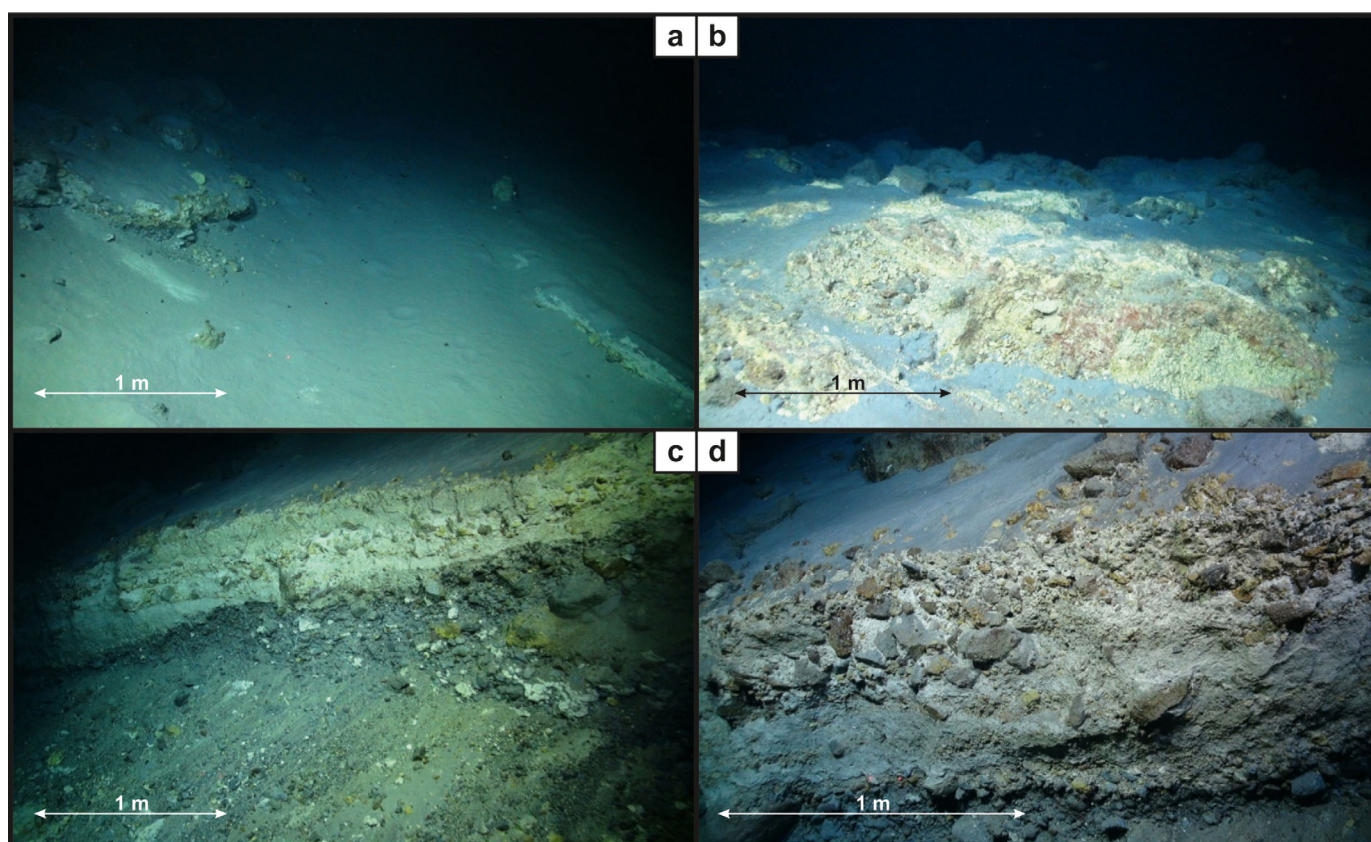


Figure 3. Images from a hummock at the northern edge of Deposit 1 (Figure 2; dive I219). (a) Patchy erosion of the hemipelagic cover over Deposit 1, providing a window into the hummock surface and exposures through the overlying sediment. (b) Top surface of hummock, showing typical exposure of hydrothermally altered volcanic rock. (c) Exposure through the sedimentary drape over Deposit 1, showing a basal layer of dense, gray, angular clasts overlain by a bedded sequence of hemipelagic sediment and mixed volcanoclastic gravel. (d) Coarse, hemipelagite-matrix-supported to clast-supported lithic breccias beds overlying the hummock surface. The basal, monomict bed of angular gray lava clasts contrasts with the overlying polymict beds.

An alternative possibility is that this unit represents a capping, coarse-grained turbidite generated by the debris avalanche; it may correlate with the gray volcanoclastic beds in the widespread 12–14 ka turbidite [cf. *Trofimovs et al.*, 2013].

3.2. Deposit 2

3.2.1. Wembley Block

The Wembley block differs from the hummocks within Deposit 1 in its scale, componentry, and shape. It also displays some differences in postemplacement sedimentary cover. Its angular, steep-sided form suggests that it is a single fragment of the volcanic edifice. The exposed base of the block is not its true base, which may be as much as 100 m below the seafloor [cf. *Crutchley et al.*, 2013].

3.2.1.1. Surface Exposures

Continuous exposures on the SE side of the Wembley block are summarized in Figure 5 (Dive I217). The lower half of the block exposes a largely structureless breccia of angular, dense, gray andesite clasts set within a uniform, white to pale-gray fine-grained matrix, which erodes with a sculpted, pitted appearance (Figures 4a, 4b, and 4f). We interpret this matrix as hemipelagic mud, because of its similar appearance to the hemipelagite exposed in scarps that cut the seafloor east of the block [this mud has been sampled in numerous cores, *Trofimovs et al.*, 2013]. The exposures change abruptly 26 m above the seafloor, to volcanic breccias of dense angular clasts, either gray or red in color, displaying crude low-angle bedding (Figure 6d), but without any pale mud matrix (Figure 5). The volcanic breccias are similar in appearance to unaltered breccias in Deposit 1, but hydrothermally altered rocks are absent. Some clasts show fractures (Figure 6e) that may reflect in situ brecciation acquired by vibration and collision during transport. Exposures vary from matrix to clast-supported breccias. Although most are monomict, some beds contain mixtures of gray and

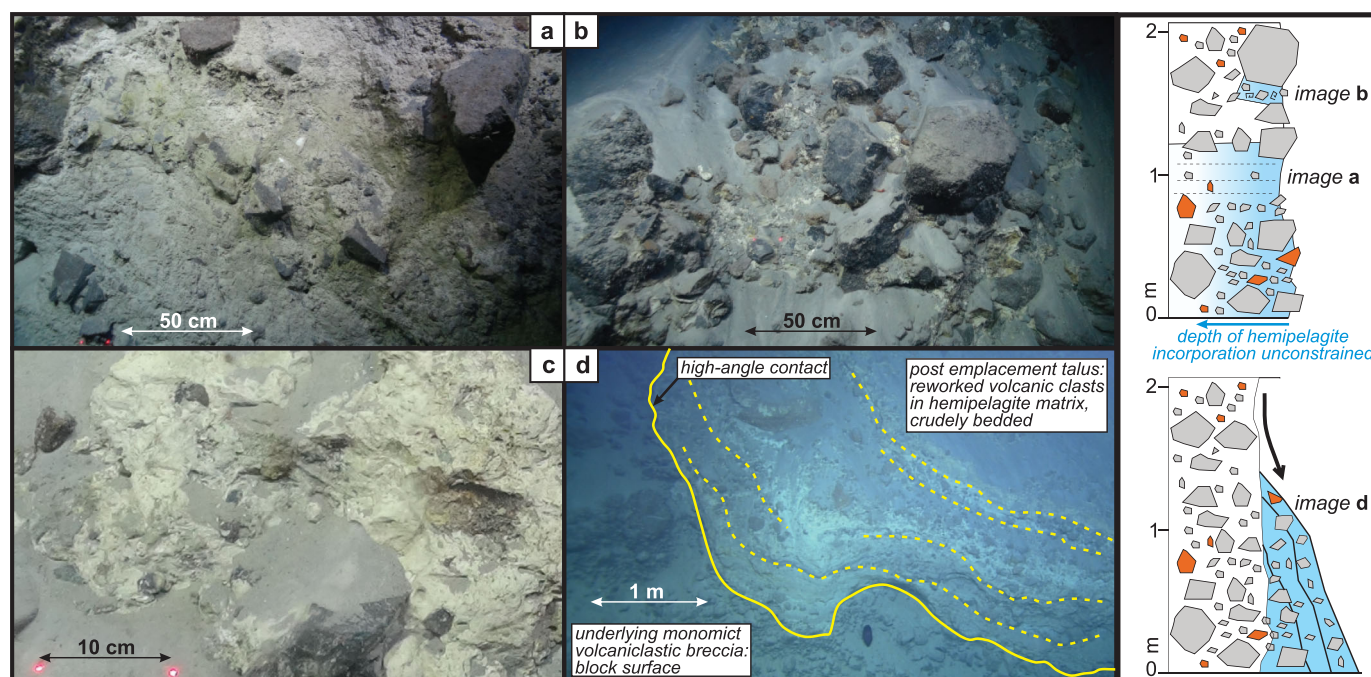


Figure 4. Images of pale fine-grained sediment, interpreted as hemipelagic mud, within exposures of the Wembley block (locations in Figure 2a). (a) Hemipelagic mud-rich interval of the block surface, near the base of the SE side of the block (position in Figure 5), with lava clasts defining crude stratification. (b) Mixed volcanoclastic breccia in the upper half of the Wembley block, comprising dense gray, red and black lava clasts (position in Figure 5). Beneath a covering of recent gray volcanoclastic sand, pale mud (center) occurs in a small isolated patch, encasing volcanic clasts. (c) Typical appearance of pale mud, with a pitted and sculpted surface, in places preserving stretched or sheared fabrics, suggestive of a cohesive, clay-rich hemipelagite. (d) Crudely bedded polymict, matrix-supported breccia of volcanic clasts embedded in a white to pale hemipelagic mud matrix (outlined in yellow), unconformably overlying a monomict clast-supported lava breccia at a high angle, at the base of the SW side of the block. The right-hand plot shows schematic interpretations of the contrasting hemipelagic-rich breccia at different exposures around the Wembley block. In Figures 4a and 4b, the hemipelagic mud appears to form a matrix to the primary lithology of the block (although how and when this is acquired is open to interpretation—see text), but in Figure 4 d it forms a postemplacement talus derived from reworked material.

red lava fragments, and are subrounded in parts. We interpret the monomict breccias as dome-collapse block-and-ash flow deposits, and the more mixed, rounded units, as reworking of the same material. The common occurrence of reddened lavas suggests a subaerial origin.

Very dark lava clasts are exposed near the base of the ESE side of the Wembley block (Dive I217). Based on samples with a similar appearance from Deposit 3, we interpret these as blocks with ferromanganese surface encrustation (Figures 4e and 6c). Such encrustation is likely to have formed after deposition, assuming that the block surfaces were not previously exposed in a submarine environment. It is unclear why this encrustation is restricted to a single part of the Wembley block, but the formation of ferromanganese crusts can be strongly dependent on water depth and local biological activity [Hodkinson and Cronan, 1991].

The base of the Wembley block on its SW side (Dive H1308) also exposes volcanic breccias within a hemipelagic mud matrix, but here they display crude, high-angle bedding, and unconformably overlie a monomict volcanic breccia without any mud matrix (Figure 4d). We interpret the bedded mud-supported breccia as a postemplacement talus of volcanic clasts mixed with continuously depositing hemipelagic sediment, derived from periodic mass wasting of the steep slopes of the Wembley block. The monomict breccia is thus the surface of the primary block. Higher up the SW side of the block, clast-supported volcanic breccias dominate (Figure 6a). Overall, these are more angular than the breccias on the SE side. We interpret the whole sequence as autoclastic and reworked lava breccias forming as talus around an active lava dome. The greater prevalence of reworked breccias on the SE side of the block suggests a more marginal facies than those on the SW, which is plausible given the 900 m dimensions of the block. The entire block is thus a fragment of the subaerial volcano, transported intact to its present position.

3.2.1.2. Seafloor Interaction

Although the mud-supported breccias on the SW side of the block are clearly postemplacement talus deposits, the mud-supported breccias on the SE side may be a syn-emplacement feature. Here the mud matrix is present on subvertical and highly irregular, gullied slopes, sometimes showing a gradational

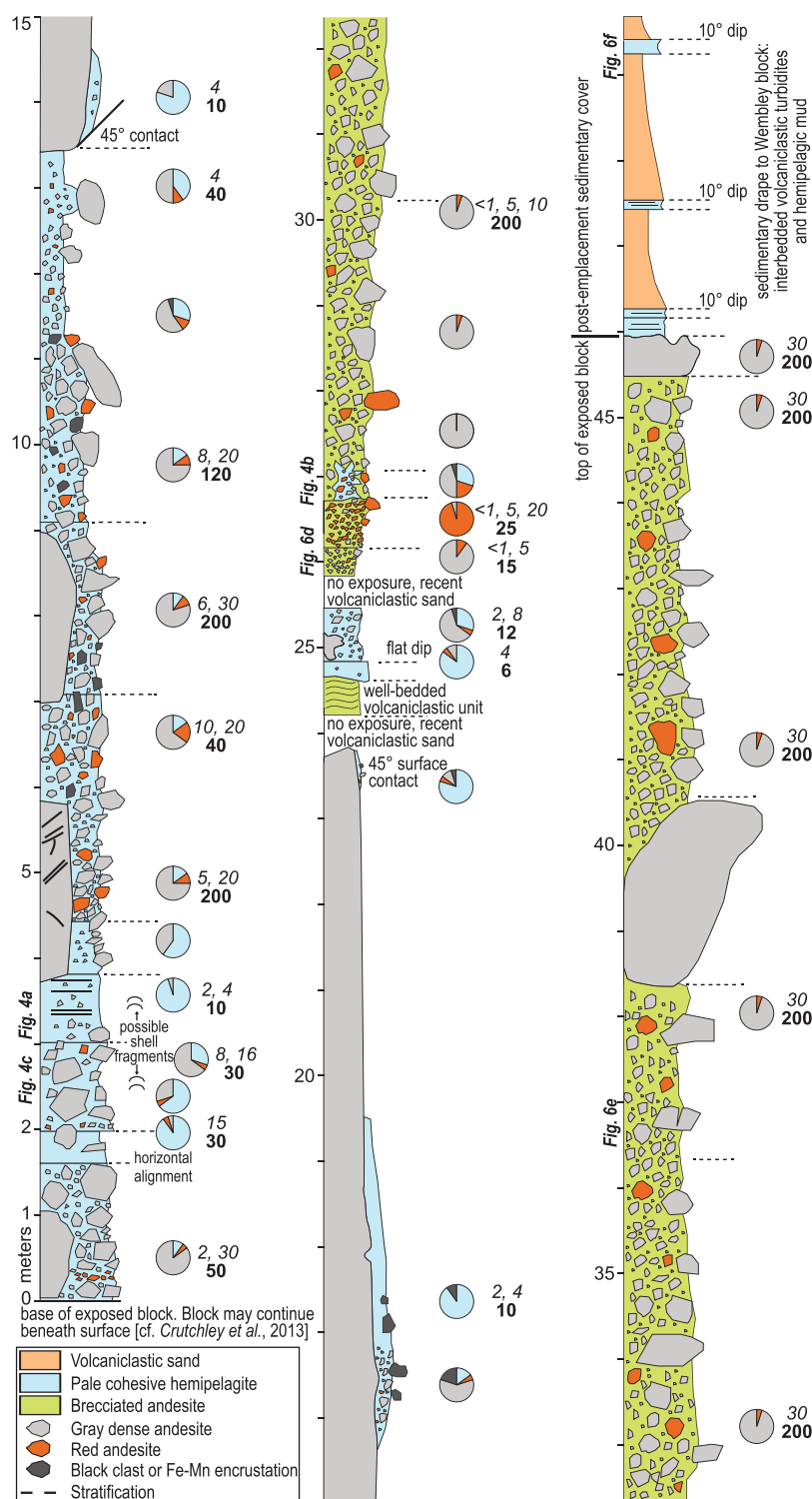


Figure 5. A visual log, reconstructed from ROV imagery, of a transect up the exposed surface on the SE side of the Wembley block (map in Figure 2). The surficial exposure may not be representative of internal stratigraphy of the block. A white cohesive material encases volcanic clasts across much of the lower half of the Wembley block, and is interpreted as hemipelagic mud. This material is rare in the upper part of the block. The uppermost part of the block exposes interbedded grey volcaniclastic sands and pale hemipelagic mud, very similar in appearance to material sampled in the JR123 vibrocores from the surrounding seafloor [Trofimovs *et al.*, 2008, 2010]. Pie charts indicate the relative proportions of exposed surface area accounted for by different components. Modal and maximum lithic clast diameters, in centimeters, are given in *italics* and **bold**, respectively (in several cases two modes are apparent).

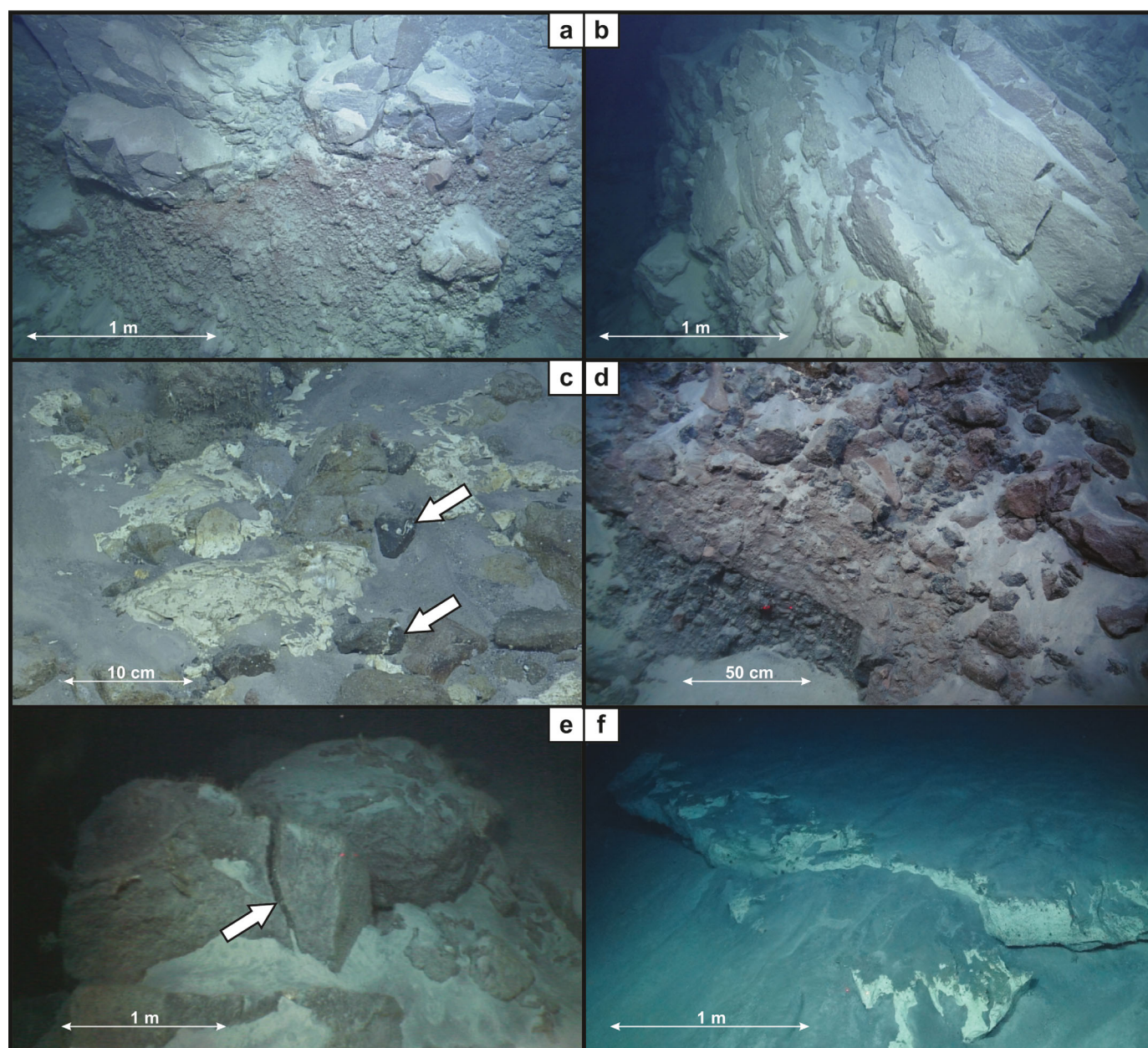


Figure 6. Images of the Wembley block lithologies (locations in Figures 2 and 5). (a) Monomictic red and gray lava breccias and massive fresh angular lava blocks. (b) Massive single lava block within side of Wembley block. (c) Massive matrix-supported breccia of volcanic clasts within a white to pale hemipelagite mud matrix. Dark coloration may be due to Fe-Mn encrustation (arrows). In some cases (lower arrow), the color contrast suggests variable encrustation in a single clast. (d) Succession of two monomictic lava breccias (black overlain by red) in the upper part of the Wembley block, interpreted as block-and-ash flow deposits. (e) Andesite boulder with jig-saw fit fracture implying impact with nearby blocks during emplacement of the Wembley block. (f) Hemipelagic mud bed exposed at the top of the Wembley block, overlying a recessive bed of volcanoclastic sand (Figure 8). Figures 6a–6c are from dive H1308, and Figures 6d–6f from I217.

contact with monomictic, clast-supported volcanic breccias (Figure 4), and is prevalent below a sharp and broadly horizontal boundary. The SE side of the block was the frontal section during block emplacement, and seismic reflection data indicate that the emplacement of Deposit 2 involved substantial erosion of sea-floor sediment [Watt *et al.*, 2012a, 2012b]. Incorporation of mud into the brecciated surface of the block may have occurred during this process, explaining the presence of this matrix in the lower and frontal part of the block. This sediment injection is not necessarily deeply penetrating. We favor this interpretation over alternative origins for the marine sediment matrix on the SE side of the Wembley block. Hemipelagic mud characterizes marine sedimentation on the deep seafloor around Montserrat; if a marine matrix was a

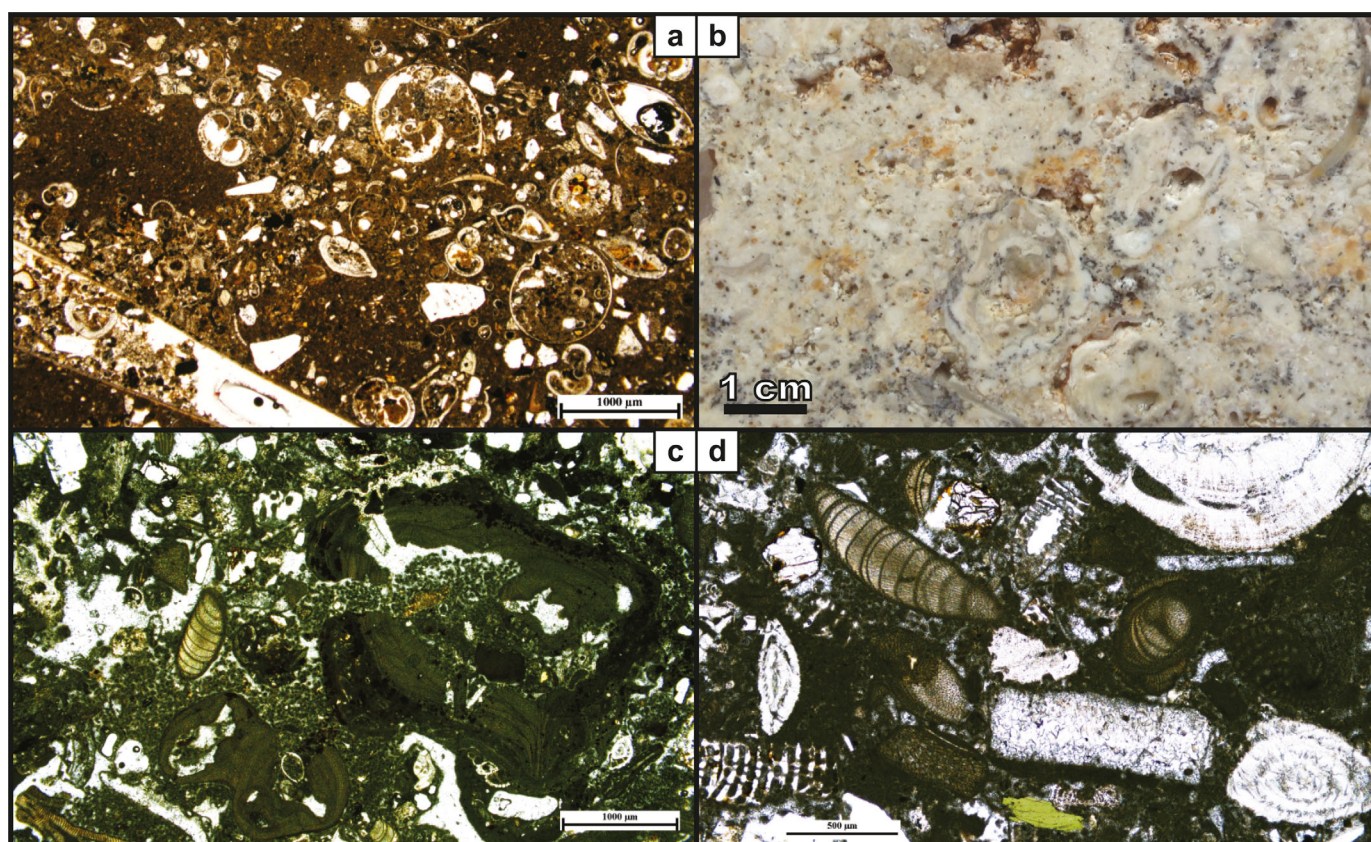


Figure 7. Images of carbonate samples (NA037-002 (975 m) and NA037-005 (942 m); Figure 1) from the Wembley block. (a) NA-37-005: a pelagic limestone comprising planktonic foraminifera (including *Globorotalia*), planktonic gastropods (heteropods and pteropods). Rounded patches of micrite with few bioclasts are likely burrow fills. Shallow-water benthic foraminifera are rare. (b) Hand specimen of NA037-002, a shallow-water limestone with rhodoliths of coralline algae and a variety of bioclasts. The same rock is shown in Figure 7c, where rhodoliths have been extensively bored by a clionid sponge, and shallow-water bioclasts including foraminifera and bivalves are present, along with abundant peloids of probable microbial origin, and in Figure 7d, where (top right) large benthic foraminifera (*Amphistegina*), (middle) coralline algae, (bottom middle) bivalve fragments (original aragonite replaced by calcite spar), and (bottom left) partially dissolved peneroplid foraminifera all occur within a matrix of micrite and calcite spar. Some volcanic crystals and rock fragments are also present.

primary characteristic of the block (and if we assume the block originated on the submerged island flanks), we would expect more evidence of shallow water carbonate rocks, and for the volcanic breccias to be more extensively reworked. Rare white fragments are observed in the hemipelagic mud (Figure 5), up to 2 cm across, but these may be deep water bivalves of the type observed (up to 0.5 cm across) on the south side of Montserrat.

3.2.1.3. Sample Descriptions

A single lava sample from the block (NA037-001; see supporting information) comprises fresh, dense porphyritic andesite with a phenocryst assemblage of plagioclase, orthopyroxene, and clinopyroxene. Hornblende is absent. This assemblage contrasts with the andesite mineralogy that has predominated on Montserrat since ~110 ka (and that occurs in Deposit 1), but is similar to rocks erupted before 130 ka [Harford *et al.*, 2002; Zellmer *et al.*, 2003].

Loose yellow clasts of highly indurated carbonate, up to 30 cm across, were observed on the block surface near the top of the SW side of the block (Dive H1308; Figure 7). A sample of this material (NA037-002; see supporting information) is a coralline limestone consisting of a mixture of large (cm-sized) rhodoliths, benthic foraminifera (notably *Amphistegina* and peneroplids), and other bioclasts (including gastropods, bivalves, echinoids, and calcareous red algal fragments) within a matrix of micrite. Microbialite-micritic filaments and peloids probably represent in situ bacterial precipitates. Some bioclasts have textures indicating replacement of original aragonite by neomorphic calcite. The characteristics of this clast suggest formation at shelfal depths, but the replacement of aragonite suggests diagenesis either in a meteoric environment or in its current deep water setting (900 m). A second sample (NA037-005) is a weakly indurated micritic limestone with planktonic foraminifera (*Globorotalia*, *Orbulina*), planktonic gastropods (including pteropods),

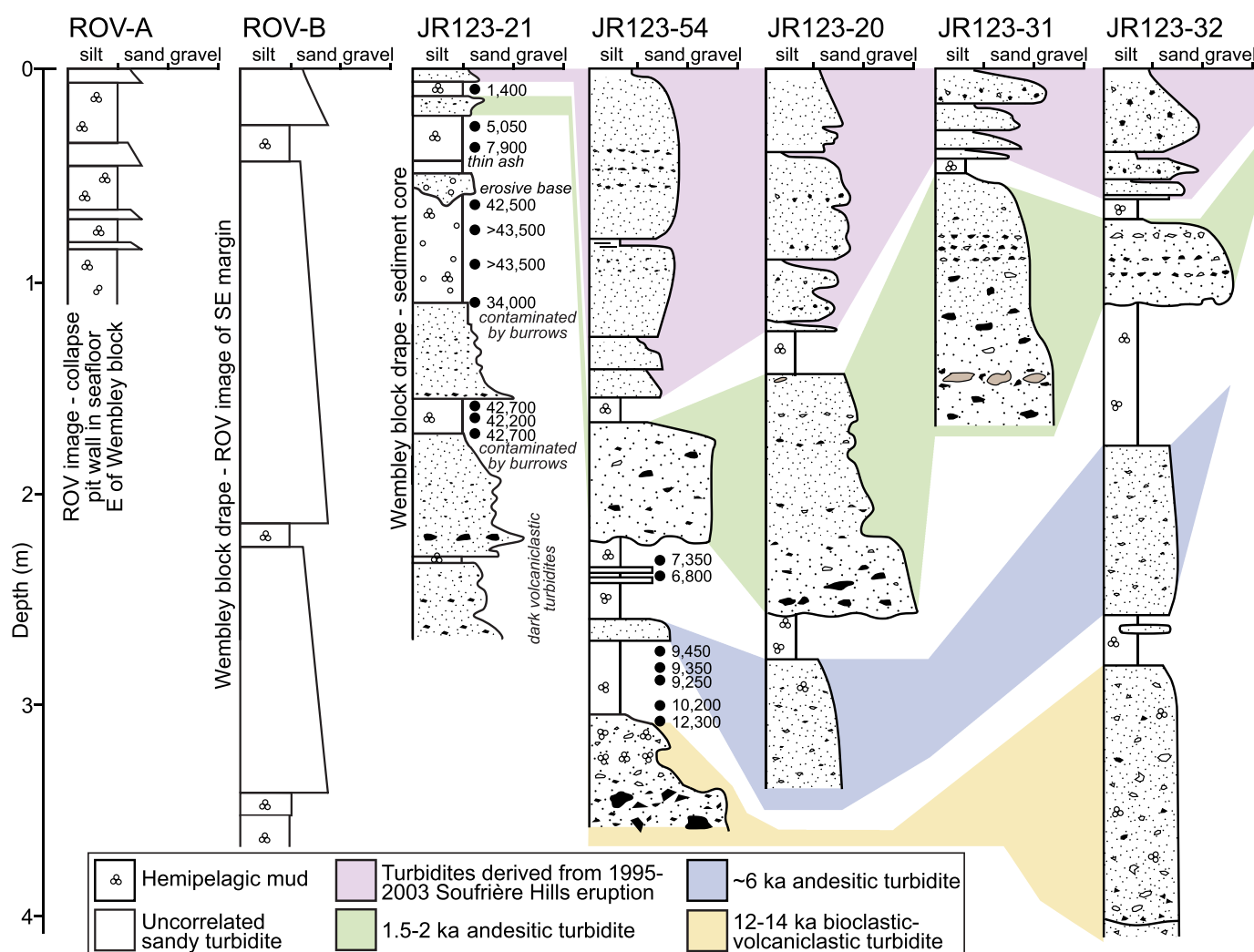


Figure 8. Stratigraphic logs and new radiocarbon dates (Table 1) of core JR123-21 taken from the top of the Wembley block (Figure 2) compared with ROV imagery from the eastern side of the Wembley block (Figure 5), an exposure through seafloor sediment to the east (Figure 11c), and stratigraphic logs of cores described in Trofimovs *et al.* [2013]. Site locations shown in Figure 2.

minor fragments of shallow-water bioclasts (bivalves, foraminifera, echinoids), and silt-sized volcanic crystals set in a micrite matrix with conspicuous (mm sized) burrow fills. The sample exterior has some tubeworm clasts and small coral fragments. The mix of shallow and deep water fauna, with incorporation of minor volcanic fragments and aragonite replacement all suggest transport from a shallow to a deeper environment. We infer that these clasts were transported from shallow water to their current position during emplacement of the Wembley block. They may represent material from the submarine shelf that was eroded during the passage of the volcanic debris avalanche, which fell onto the surface of the block before being transported to their present position.

3.2.2. Large Southern Block

A large block south of Deposit 1, mapped as a marginal block within Deposit 2 (Figure 1, Dive I213) [Watt *et al.*, 2012b], comprises monomict lava breccias with dark coloration, interpreted as ferromanganese encrustation. Gray volcaniclastic sand from the recent Soufrière Hills eruption obscures much of the block surface. Our limited observations suggest that the block is lithologically similar to the Wembley block.

3.2.3. Wembley Block Sedimentary Drape

Approximately 3 m of marine sediment is exposed on top of the SE side of the Wembley block (Figure 5). Prominent beds of white hemipelagic mud are interbedded with three thicker, recessive gray sandy units, interpreted as turbidites, which are partly obscured by deposits of recent volcaniclastic sand (Figure 6f).

In comparison with the stratigraphy of core JR123-21, collected on top of the Wembley block in 2005 [Trofimovs *et al.*, 2008, 2010], the drape on the SE edge of the block contains thicker turbidites and thinner hemipelagite intervals (Figure 8). Both sequences are very different in terms of both layer thickness and characteristics from the stratigraphy recovered in over 20 vibracores from the surrounding seafloor (JR123) [Trofimovs *et al.*, 2008, 2010, 2013] (Figure 8).

The youngest turbidites in the correlated stratigraphy from the surrounding seafloor are much thicker than those from JR123-21. This may be explained by the elevated position of the block, where clast concentration in turbidity currents may have been lower (resulting in thinner deposits). However, the sandy beds at the base of JR123-21 are notably thick. These lower units are almost purely volcanoclastic, and do not correlate clearly with any turbidites in the local stratigraphy, which is well defined at ages <110 ka [Trofimovs *et al.*, 2013]. They may be the deposits of older turbidity currents generated during the emplacement of Deposit 2.

The Wembley block is mapped as part of Deposit 2 [Watt *et al.*, 2012a, 2012b; Crutchley *et al.*, 2013], but its location (Figure 1) suggests that it could be an outrunner block within Deposit 1. Seismic reflection profiles and the regional turbidite record provide no evidence of major landslides in the period between Deposits 2 (~130 ka) and Deposit 1 (11.5–14 ka). New radiocarbon dates from JR123-21 (Figure 8 and Table 1) extend beyond the limits of radiocarbon dating (43.5 ka), supporting interpretation of the Wembley block as part of Deposit 2. However, the dates do not provide good constraints on turbidite ages or hemipelagic sedimentation rates, because several ages cluster around 43 ka, and some are out of stratigraphic sequence (Figure 8). This suggests extensive bioturbation or the possible reworking of material derived from bioclastic turbidites with background hemipelagic sediment. The 1.2 m thickness of hemipelagic intervals in JR123-21 also supports a pre-Deposit 1 age for the Wembley block: post-Deposit 1 hemipelagic mud on the surrounding seafloor has a cumulative thickness of 70–80 cm; and hemipelagic sedimentation rates of 6.6 cm kyr⁻¹, estimated from a 45 cm vibrocore (JC83-VC1) on top of the large southern block (Figure 1 and Table 1) imply that the hemipelagite in JR123-21 represents >18 kyr. However, the sedimentary drape is surprisingly thin if the emplacement age of the block is 130 ka. Thus, although the balance of observations suggests that the Wembley block lies within Deposit 2, several aspects of the sedimentary drape remain puzzling.

3.3. Deposit 3

The surface of Deposit 3 (Dive H1310; Figure 1) is not well exposed, but occasional clusters of meter-scale blocks, with features such as well-developed radial jointing (Figure 9a), protrude through younger sedimentary cover. The blocks are dense porphyritic andesite lavas with a very dark surface coating, caused by thick (up to 3 mm) manganese encrustations. Examination of two thin sections (NA037-037 and NA037-042; supporting information) indicates a phenocryst assemblage of plagioclase, clinopyroxene, and orthopyroxene. Orthopyroxene is less abundant than in the Wembley block sample (NA037-001). The assemblage is comparable to that observed in the pre-130 ka andesites of Soufrière Hills and in some of South Soufrière Hills rocks [Zellmer *et al.*, 2003], although olivine is absent. An origin from South Soufrière Hills would be consistent the previous correlation of Deposit 3 with a mafic volcanoclastic turbidite [Cassidy *et al.*, 2014]. The prevalence of angular, fractured lava blocks suggests a subaerial source for the landslide; the absence of a visible source scar and a lack hydrothermally altered material in the exposures suggests that this landslide may have been relatively shallow-seated.

3.4. Deposit 5

Clusters of blocks in Deposit 5 are well exposed at depths of 750–830 m (Dive H1309; Figure 1). Blocks comprise massive carbonate fragments (Figure 9f) and well-bedded carbonate-cemented volcanoclastic conglomerates. The well-rounded conglomerates (Figure 9c) are comparable to beach cobbles and mature fluvial deposits, and the carbonate fragments are similar to large slabs of hardground observed in separate dives at depths of 100–200 m off the southern coast of Montserrat. A single large slab of reef rock has karstic features (deeply incised channels) indicative of subaerial exposure, perhaps during a low stand in sea level (Figures 9d and 9e).

One carbonate sample (NA037-026; Figure 10, supporting information) is a dense limestone of encrusted volcanic clasts and bioclasts, including benthic and planktonic foraminifera, calcareous red algae, mollusc fragments, serpulids, sponge spicules, radiolaria, echinoid spines, and pteropods, cemented by micritic-microsparitic-sparry

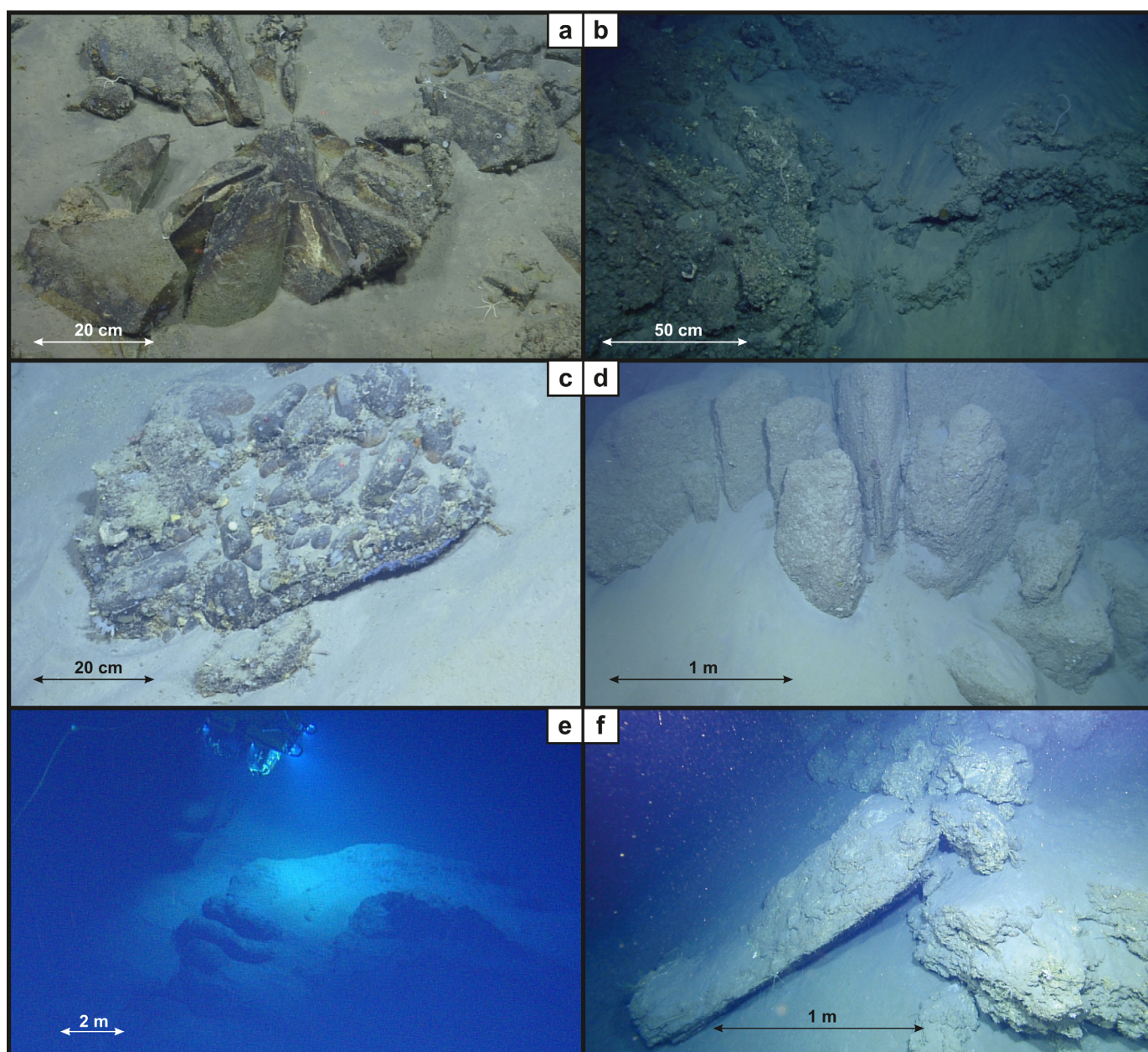


Figure 9. Images of block exposures in Deposits 3 and 5 (Figure 1; dives H1309 and H1310). (a) Radially fractured dense lava block with dark Fe-Mn encrustation. This is the dominant lithology exposed at the surface of Deposit 3. (b) Polymict breccias of altered subangular and scoriaceous volcanic clasts, forming a possible surficial deposit overlying Deposit 3. (c) Carbonate cemented conglomerate of rounded lava cobbles (beach type rock) in Deposit 5. (d) Karstic weathering in a reef block in Deposit 5. Field of view ~ 3 m. (e) An overhead view of a weathered carbonate reef block in Deposit 5. (f) Slab-like carbonate blocks within Deposit 5. Similar lithologies were observed on the SW flank of Montserrat, encrusting the submerged flank of the island.

calcite cement. The encrusted grains (comparable to oncoids or rhodoliths) probably formed by rolling in intermittent currents in shallow to moderate water environments, consistent with the fossil assemblage. Encrusting foraminifera on red algal crust occur with microbial filaments. Aragonitic gastropod and sponge fragments are replaced by coarse calcite, consistent with diagenetic alteration following transport to a deep water environment. Phosphate grains of probable microbial origin occur within cavities (sponge borings) in calcareous algae. A further sample (NA037-025) is a well-sorted, porous cemented bioclastic grainstone (medium to coarse sand) cemented by thin (20–50 μm) isopachous bladed calcite. Grains include shallow-water foraminifera (penerolids), calcareous algae (branched forms), green algae (*Halimeda*), minor bivalve fragments, and volcanic clasts. Areas of peloidal sediment are likely to be the result of bacterial precipitation. Our observations support the previous

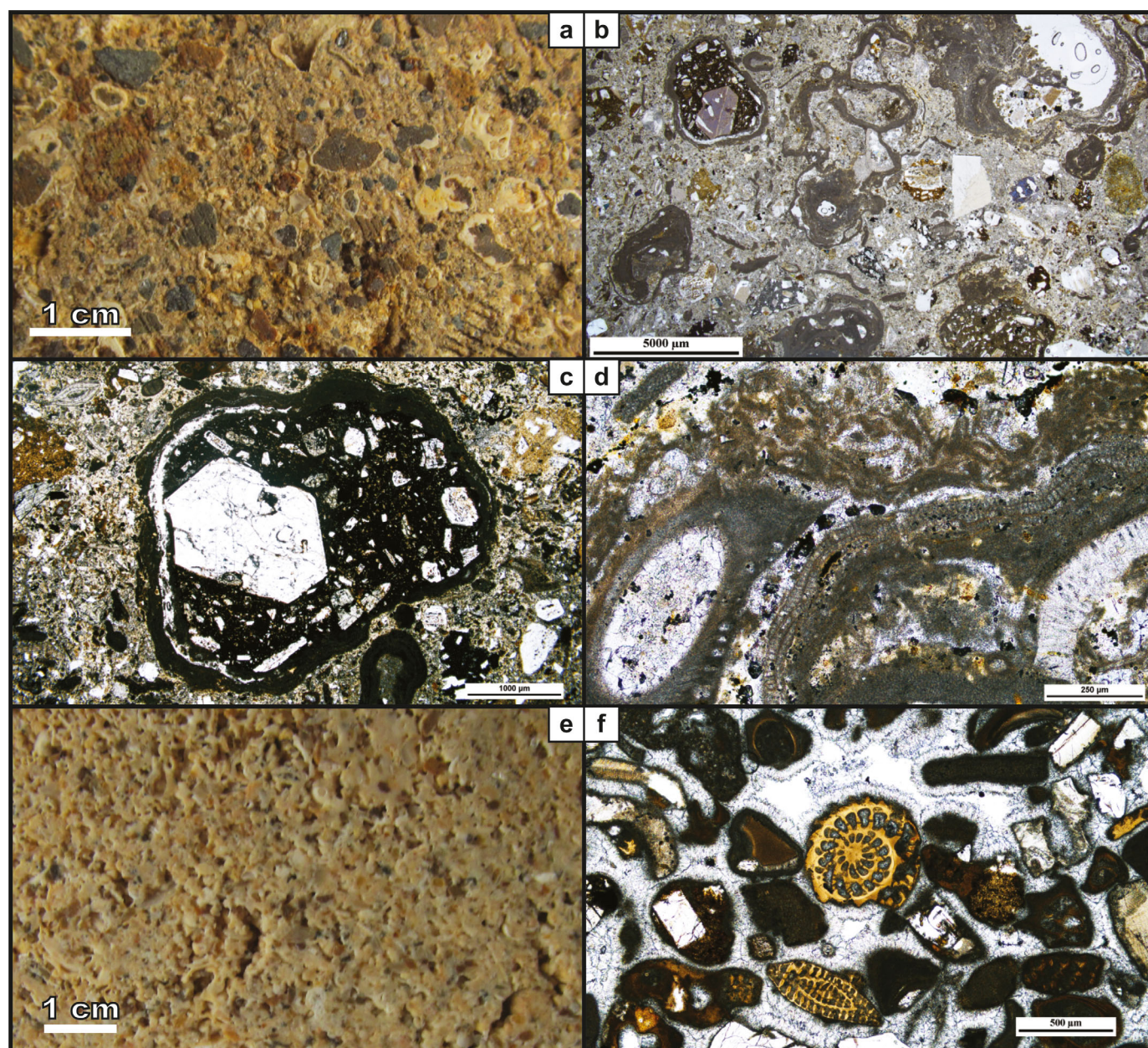


Figure 10. Images of carbonate samples (NA037-025 (806 m) and NA037-026 (823 m); Figure 1) from Deposit 5. (a) NA037-026, a limestone comprising coated rounded and subangular volcanic clasts in a carbonate matrix. In Figure 10b, the coating is shown to comprise a mixture of calcareous algae and other biota, whereas the surrounding matrix contains fine-grained volcanic material, micrite, and calcite spar. A similar matrix and algal-coated grain is shown in Figure 10c, as well as shallow-water fossils (e.g., benthic foraminifera *Amphistegina*, top left). The coating in sample NA037-026 is shown in more detail in Figure 10d, where an algae nodule is encrusted by foraminifera, serpulid and microbial filaments. Sponge spicules occur in the surrounding matrix. (e) NA037-025, a well-sorted bioclastic grainstone, comprising bioclasts and minor volcanic grains cemented by an isopachous fibrous calcite fringe (f). Bioclasts include peneroplid foraminifera, coralline algae, and bivalve fragments.

conclusion [Le Friant *et al.*, 2004; Cassidy *et al.*, 2013] that Deposit 5 originated as a shallow-seated collapse of the coastal shelf.

3.5. Sharp-Faced Depressions in Young Sediment

Numerous sharp-faced depressions, up to a few meters deep, occur on the seafloor between hummocks in Deposit 5 and to the east of Deposit 1 [cf. Watt *et al.*, 2012b]. These structures are defined by arcuate scarps, in some cases forming fully enclosed, round depressions, exposing near-vertical cliffs through the seafloor sedimentary sequence (Figures 11b and 11c). The depressions are at least tens of meters across in the

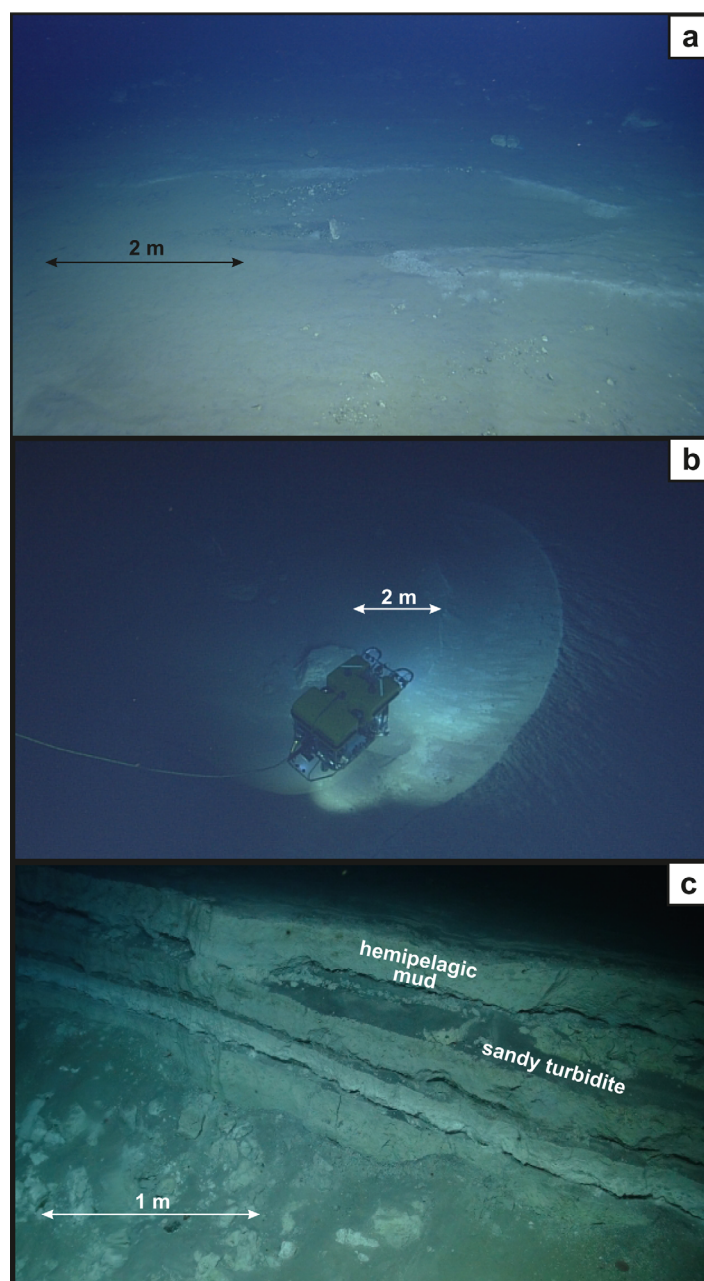


Figure 11. ROV images of circular erosional or collapse structures forming within young seafloor sediment (locations in Figures 1 and 2). (a) Shallow dish-like pockmarks in Deposit 5, cutting a scarp in hemipelagic sediment all around the margin. (b) Overhead view of a relatively deep (~5 m) pockmark in Deposit 5. A sharp, circular wall marks positive relief beyond the margin of the structure, with a streaking, radiating pattern on the seafloor outside the structure. The wall cuts steeply through seafloor strata of interbedded hemipelagic and volcanoclastic sand. (c) Pockmark wall beyond the margin of Deposit 1, east of the Wembley block, and overlying part of Deposit 2 (Figure 1). This seafloor stratigraphy is exposed, showing four distinct hemipelagic layers, present throughout the region in cores collected in JR123 [Trofimovs *et al.*, 2008, 2010] (Figure 8). Exposure of these young depositional layers suggests recent erosion.

4.1.1. Subaerial Source Region

English's Crater and the Tar River Valley display two volcanic facies [Harford *et al.*, 2002]: near-vertical walls of massive lava crop out to the west (Chances Peak; age unknown) and south (Galways Mountain, 112 ka; Perches Dome, 24 ka); and radiating fans of crudely bedded lava breccias (rock fall and block-and-ash flow

vicinity of Deposit 5, and up to hundreds of meters across to the east of Deposit 1. The stratigraphy of scarps east of Deposit 1 (Figure 11c) comprises interbedded turbidites and hemipelagic mud but is difficult to correlate precisely with the regional turbidite stratigraphy (Figure 8). The good exposure of the scarps suggests that they cut through to the youngest Holocene deposits and that they therefore formed (or have been actively eroded) very recently.

The spatial distribution of the depressions and their fully enclosed shapes suggests that they are not simply scour structures, but have a genetic relationship with debris-avalanche deposition. The depressions east of Deposit 1 lie in a region where failure of the preexisting seafloor sediment occurred during the Deposit 2 landslide [Watt *et al.*, 2012b; Crutchley *et al.*, 2013]. The structures may be collapse pits in younger sediment produced by seafloor subsidence or fluid venting driven by compaction within the underlying landslide deposit.

4. Implications for Landslide Processes

4.1. The Source and Composition of Deposit 1

The rocks exposed in Deposit 1 include near-vent and subaerial lithologies, consistent with English's Crater being the major source of material in the deposit. This correlation places an age of 11.5–14 ka on the formation of English's Crater, which is significantly older than the 6 ka minimum age provided by dates of infilling deposits [Smith *et al.*, 2007; Boudon *et al.*, 2007].

deposits) crop out at the northern and lower margin of English's Crater and along the Tar River Valley. Block-and-ash flow deposits on the east coast, south of Spanish Point, have radiocarbon ages of 19.7 and 24.0 ka [Roobol and Smith, 1998] and can be traced toward English's Crater. They may be associated with Perches Dome, given their similar age. Similar lava breccias between Chances Peak and Galways Mountain, as well as deposits dated at 16–19 ka on the west side of the island, in Fort Ghaut, suggest elevated levels of extrusive volcanism on Montserrat between 16 and 24 ka. However, the remains of Perches dome are the only exposed Soufrière Hills lavas from this time period. It is possible that a much more extensive lava-dome complex of this age formed the source of the Deposit 1 landslide, also removing sections of massive lava from older domes to form the near-vertical cliffs currently exposed around English's Crater. A relatively deep-seated collapse, centered on the vent region, is supported by the high proportion of hydrothermally altered material in Deposit 1. At least three extensive fumarole and hot spring systems existed inside English's Crater prior to 1995 (Lang's, Cow Hill New, and Tar River), providing evidence of intense hydrothermal activity in this area [Roobol and Smith, 1998].

4.1.2. Incorporation of Submarine Material

A single observation of a clast (Figure 2f) with contrasting surfaces of fresh andesite and weathered, tube-worm encrusted andesite, provides the only direct evidence for the incorporation of submarine material within Deposit 1. This conflicts with morphological observations: the maximum plausible subaerial failure volume of $\sim 1 \text{ km}^3$, based on combining the Tar River Valley and English's Crater depressions, with prefailure elevations of $> 1100 \text{ m}$, is too small to account for the volume of Deposit 1 (1.7 km^3). The chute cut into Montserrat's eastern flank also suggests that submerged material formed part of the landslide. Such material would likely comprise carbonate and reworked, polymict volcanic clasts. The absence of these lithologies suggests that the surface exposures of Deposit 1 may not be representative of the deposit as a whole.

The correlation of Deposit 1 with the large-volume 12–14 ka turbidite east of Montserrat [Trofimovs *et al.*, 2013] (see section 2.3.1) also implies a submarine component to the event. The turbidite comprises approximately equal proportions of volcanoclastic and bioclastic grains, in contrast to the entirely volcanic lithologies exposed in Deposit 1. If the two events are related, then the bioclastic component of the turbidite must derive from seafloor material disaggregated during landslide emplacement. The shelf chute aligned with Deposit 1 provides supporting evidence of such a process. Given the absence of submarine lithologies within surface exposures of the Deposit 1 hummocks, the submarine component of the landslide may be concentrated disproportionately within the unexposed matrix facies between the debris-avalanche deposit hummocks.

4.2. Emplacement Mechanisms and Comparison With Subaerial Debris-Avalanche Deposits

4.2.1. Deposit Morphologies

Deposit 1 is morphologically and texturally similar to many subaerial debris-avalanche deposits. The rounded hummocks of the deposit, comprising heterogeneous mixtures of deformed and frequently altered monomict domains, are typical of many subaerial examples [e.g., Glicken, 1996; Shea *et al.*, 2008; Clavero *et al.*, 2002]. The fan-shaped morphology of Deposit 1 is comparable to freely spreading deposits such as those at Galunggung and Mombacho volcanoes [Siebert, 1984; Shea *et al.*, 2008], and indicative of granular avalanche emplacement processes [cf. Paguican *et al.*, 2014]. Landslide mobility indices [cf. Griswold and Iverson, 2008; Iverson *et al.*, 2015] for Deposit 1 are also within the range of typical values for subaerial volcanic debris avalanches ($L/H = 7$ and $A/V^{2/3} = 36$, based on parameters in Lebas *et al.* [2011]) [Legros, 2002; Griswold and Iverson, 2008].

In contrast to Deposit 1, Deposit 2 forms a continuous elongate deposit, and its mobility is at the high end of the range defined by subaerial volcanic debris avalanches ($L/H = 16$ and $A/V^{2/3} = 47$, based on parameters in Watt *et al.* [2012b]), which partly reflects the incorporation and secondary failure of large volumes of seafloor-sediment within the deposit [cf. Watt *et al.*, 2012a, 2012b]. Deposit 2 has a central thickness of over 100 m, and a surface marked by isolated blocks set within the more continuous landslide mass (as indicated by seismic reflection profiles [Crutchley *et al.*, 2013]). Although this mass may be disaggregated and mixed, the blocks are competent, intact fragments of the initial volcanic failure region. They are hundreds of meters across, and have subvertical sides that reach over 100 m in height. Observations of the Wembley block and a large block to the south show that they comprise bedded sequences of volcanoclastic breccia, suggestive of marginal and probably near-surface portions of a subaerial lava-dome complex. The blocks result in a

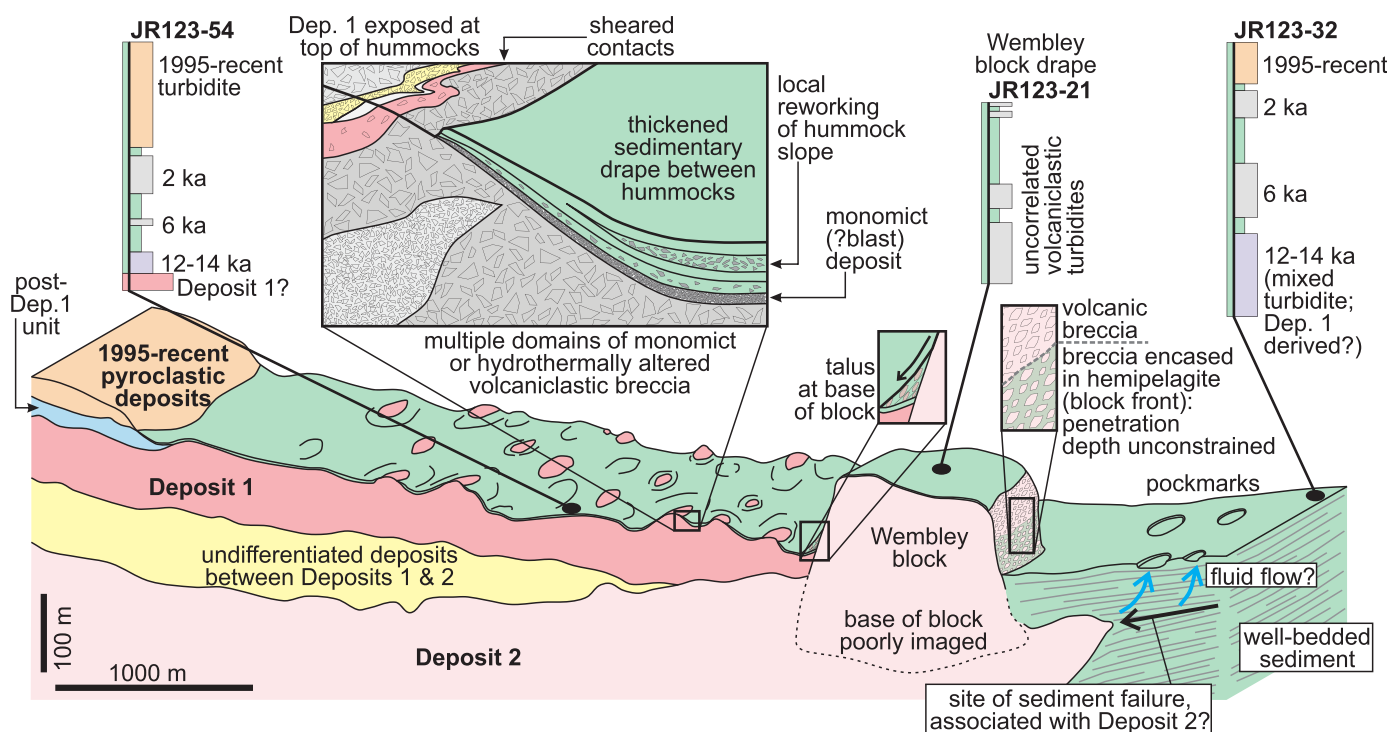


Figure 12. A schematic cross section through the landslide deposits east of Soufrière Hills, Montserrat, summarizing the main observations made for Deposits 1 and 2 in this study. The vertical section and scale are based on seismic profiles through the deposits [cf. Crutchley et al., 2013; Karstens et al., 2013].

prominent morphological front within the thick, central part of Deposit 2 [Watt et al., 2012b]; the well-exposed southern blocks are closely aligned with the southern lateral margin of the deposit, and the Wembley block lies near the northern margin (Figure 1). The deposit morphology is similar to the Icod debris-avalanche deposit, north of Tenerife [Masson et al., 2002], which has several kilometer-scale blocks at its lateral margins. Masson et al. [2002] conclude that the Icod deposit shape and block distribution is characteristic of coarse-grained debris flow processes [cf. Major and Iverson, 1999], and suggest that this behavior reflects the high proportion of pyroclastic material in the landslide. Our observations do not show evidence that the Deposit 2 failure mass was significantly different to that of Deposit 1, or was rich in friable pyroclastic material, but there is good evidence of extensive seafloor-sediment failure concomitant with the volcanic landslide [cf. Watt et al., 2012a, 2012b]. This potentially produced a mixed landslide, with high proportions of fine-grained, clay-rich material.

4.2.2. Large-Block Transport

Hummocks in subaerial debris-avalanche deposits are frequently cored by large, deformed blocks of the failure mass [Crandell et al., 1984; Glicken, 1991; Paguican et al., 2014]. Partial disaggregation, extensional faulting, and shearing of these blocks produces the broadly rounded hummock form. The large blocks of Deposit 2 differ from these hummocks in that they have undergone no deformation beyond the initial fragmentation that produced them. The vertical sides, and angular, upright form of the Deposit 2 blocks, as well as their relatively long transport distance, also contrasts with Toreva blocks, which occur in proximal regions of some debris-avalanche deposits and are often rotated, with a morphology that reflects the extensional failure planes of the fragmenting mass [Siebe et al., 1992; Wadge et al., 1995; Paguican et al., 2014].

The bedded breccias that characterize the Deposit 2 blocks might be expected to disaggregate relatively readily in a debris avalanche. Their preservation as intact fragments of the failure mass may therefore be evidence of an emplacement mechanism that limited block interaction and basal deformation (at least for the small number of outsized blocks near the deposit margins), and may also reflect damping of block collision in the aqueous environment [cf. De Blasio, 2013]. Volcanoclastic breccias, as massive and bedded units, also characterize the megablocks in landslide deposits north of Oahu, Hawaii [Yokose, 2002], although the failure and transport mechanism is not necessarily similar to that of Deposit 2. Seismic reflection profiles

show that the Deposit 2 blocks are rooted within a continuous landslide deposit (Figure 12), suggesting that block emplacement is not explained by low-friction transport of individual fragments on a lubricated basal surface of wet sediment [i.e., as characterizes isolated outrunner blocks in some submarine rock avalanches, *De Blasio et al.*, 2006; *De Blasio*, 2013]. Rather, the blocks appear to have been passively rafted within the main landslide mass, without any clear evidence for rotation around a horizontal axis, and pushed toward the margins during continued landslide movement [cf. *Major and Iverson*, 1999]. The lack of subaerial volcanic-debris-avalanche analogues for outsized intact blocks such as those in Deposit 2 may indicate that the development of debris-avalanche masses with sufficient proportions of fine-grained, water-saturated sediment to maintain elevated pore fluid pressures may be more easily acquired in a submarine environment, via mixing and entrainment of marine sediment.

5. Summary and Conclusions

This study presents results of the first detailed ROV investigations of multiple submerged landslide deposits around an island-arc volcano. Coupled with other methods of investigation, such as coring, bathymetric mapping, and geophysical data, the direct observations offered by ROVs significantly strengthen the interpretation of the sources of material and the processes operating during the emplacement of large landslides around volcanic islands.

Our observations indicate that Deposit 1 (1.7 km³) is similar to many subaerial volcanic debris-avalanche deposits, and is dominated by hydrothermally altered material likely to have originated from a collapse of the near-vent region of the Soufrière Hills volcano. This is surprising, given the large proportion of bioclastic material in a turbidite that correlates stratigraphically with Deposit 1, and a submerged eroded chute associated with the event. However, we infer that the bioclastic component within the turbidite is predominantly derived from preexisting seafloor sediment disrupted by the emplacement of Deposit 1 and eroded by associated turbidity currents. Our observations suggest that Deposit 1 occurred at 11.5–14 ka through the collapse of altered lava domes erupted at 16–24 ka, the relics of which form Perches Dome.

A much larger (10 km³) landslide occurred at ~130 ka, forming Deposit 2. Although this deposit was mostly inaccessible to ROV observation, we were able to study a large block of volcanoclastic breccias that represents a single intact fragment of the subaerial volcano. Its petrology is consistent with pre-130 ka Montserrat lavas. The lower part of the block exposes breccia set within a hemipelagic mud matrix, which was most likely acquired through vigorous erosion of preexisting seafloor sediment during block transport. The intact, outsized blocks within Deposit 2 were rafted within a relatively mobile debris-avalanche mass, and are best exposed near the margins of this elongate deposit.

Two landslide deposits to the south of Montserrat have very different source lithologies. Deposit 3 is morphologically similar to Deposit 1, but comprises fresher, denser lavas. We infer that it results from a shallower seated collapse, rather than a landslide that cut deeply into a hydrothermally altered edifice. This is consistent with the absence of a prominent source scar for the deposit. Deposit 5 is dominated by blocks of reef rock, and demonstrates that large landslides on the flanks of volcanic islands may occur without involvement of the active volcanic edifice, but can arise from instabilities on the carbonate-dominated shelves that may form around these islands.

References

- Belousov, A., B. Voight, and M. Belousova (2007), Directed blasts and blast-generated pyroclastic density currents: A comparison of the Bezymianny 1956, Mount St Helens 1980, and Soufrière Hills, Montserrat, 1997 eruptions and deposits, *Bull. Volcanol.*, **69**, 701–740.
- Bogoyavlenskaya, G. E., O. A. Braitseva, I. V. Melekestsev, V. Y. Kiriyanov, and C. D. Miller (1985), Catastrophic eruptions of the directed-blast type at Mount St. Helens, Bezymianny and Shiveluch volcanoes, *J. Geodyn.*, **3**, 189–218.
- Boudon, G., A. Le Friant, J. C. Komorowski, C. Deplus, and M. P. Semet (2007), Volcano flank instability in the Lesser Antilles Arc: Diversity of scale, processes, and temporal recurrence, *J. Geophys. Res.*, **112**, B08205, doi:10.1029/2006JB004674.
- Bronk Ramsey, C. (2009), Bayesian analysis of radiocarbon dates, *Radiocarbon*, **51**, 337–360.
- Carey, S., et al. (2014), Impact of volcanic eruptions on the seafloor around Montserrat, West Indies, *Oceanography*, **27**, 36–37.
- Cassidy, M., J. Trofimovs, M. R. Palmer, P. J. Talling, S. F. L. Watt, S. G. Moreton, and R. N. Taylor (2013), Timing and emplacement dynamics of newly recognised mass flow deposits at ~8–12 ka offshore Soufrière Hills volcano, Montserrat: How submarine stratigraphy can complement subaerial eruption histories, *J. Volcanol. Geotherm. Res.*, **253**, 1–14.
- Cassidy, M., J. Trofimovs, S. F. L. Watt, M. R. Palmer, R. N. Taylor, T. M. Gernon, P. J. Talling, and A. Le Friant (2014), Multi-stage collapse events in the South Soufrière Hills recorded in marine sediment cores, in *The Eruption of Soufrière Hills Volcano, Montserrat From 2000 to 2010*, *Mem. Geol. Soc. London* **39**, edited by G. Wadge, R. E. A. Robertson, and B. Voight, pp. 383–397, Geol. Soc. of London, London, U. K.

Acknowledgments

We thank Michelle Coombs and James Vallance for their constructive reviews of this work. We acknowledge support from the Natural Environment Research Council (NERC) (SFLW: NE/I02044X/1 and NE/K000403/1; PJT: ISIS research cruise JC83 (NE/0176581), NE/F010478/1 and Radiocarbon Facility allocation 1759.1013), the National Oceanic and Atmospheric Administration (NOAA) and the Ocean Exploration Trust (OET) (Cruise NA037 of the E/V Nautilus), the European Research Council (VOLDIEs project), and the Swiss National Science Foundation (MJ: PBSKP2-145907). Data relating to this work are available from the following sources: ROV data from NA037 by request through the Inner Space Center at the Graduate School of Oceanography, University of Rhode Island, USA (Dwight Coleman: dcoleman@gso.uri.edu); ROV data from JC83 from Peter Talling at the National Oceanography Centre, Southampton, UK (peter.talling@noc.ac.uk).

- Cassidy, M., et al. (2015), Rapid onset of mafic magmatism facilitated by volcanic edifice collapse, *Geophys. Res. Lett.*, doi:10.1002/2015GL064519, in press.
- Clavero, J., R. S. J. Sparks, H. E. Huppert, and W. B. Dade (2002), Geological constraints on the emplacement mechanism of the Paríacota debris avalanche, northern Chile, *Bull. Volcanol.*, *64*, 3–20.
- Clavero, J., R. S. J. Sparks, M. S. Pringle, E. Polanco, and M. C. Gardeweg (2004), Evolution and volcanic hazards of Taapaca Volcanic Complex, Central Andes of Northern Chile, *J. Geol. Soc.*, *161*, 1–17.
- Coombs, M. L., D. A. Clague, G. F. Moore, and B. L. Cousens (2004), Growth and collapse of Waianae Volcano, Hawaii, as revealed by exploration of its submarine flanks, *Geochem. Geophys. Geosyst.*, *5*, Q08006, doi:10.1029/2004GC000717.
- Coombs, M. L., S. M. White, and D. W. Scholl (2007), Massive edifice failure at Aleutian arc volcanoes, *Earth Planet. Sci. Lett.*, *256*, 403–418.
- Crandell, D. R., C. D. Miller, H. X. Glicken, R. L. Christiansen, and C. G. Newhall (1984), Catastrophic debris avalanche from ancestral Mount Shasta volcano, California, *Geology*, *12*, 143–146.
- Croff Bell, K., S. N. Carey, P. Nomikou, H. Sigurdsson, and D. Sakellariou (2013), Submarine evidence of a debris-avalanche deposit on the eastern slope of Santorini volcano, Greece, *Tectonophysics*, *597–598*, 147–160.
- Crutchley, G. J., et al. (2013), Insights into the emplacement dynamics of volcanic debris avalanches from high resolution 3D seismic data offshore Montserrat, Lesser Antilles, *Mar. Geol.*, *335*, 1–15.
- Day, S., P. Llanes, E. Silver, G. Hoffmann, S. Ward, and N. Driscoll (2015), Submarine landslide deposits of the historical lateral collapse of Ritter Island, Papua New Guinea, *Mar. Pet. Geol.*, *67*, 419–438, doi:10.1016/j.marpetgeo.2015.05.017.
- De Blasio, F. V. (2013), Dynamics, velocity and run-out of subaqueous rock avalanches, *Landslide Sci. Pract.*, *5*, 57–63.
- De Blasio, F. V., L. E. Engvik, and A. Elverhøi (2006), Sliding of outrunner blocks from submarine landslides, *Geophys. Res. Lett.*, *33*, L06614, doi:10.1029/2005GL025165.
- Deplus, C., A. Le Friant, G. Boudon, J. C. Komorowski, B. Villemant, C. Harford, J. Ségoufin, and J. L. Cheminée (2001), Submarine evidence for large-scale debris avalanches in the Lesser Antilles Arc, *Earth Planet. Sci. Lett.*, *192*, 145–157.
- Dufresne, A., and T. R. Davies (2009), Longitudinal ridges in mass movement deposits, *Geomorphology*, *105*, 171–181.
- Glicken, H. (1991), Sedimentary architecture of large volcanic-debris avalanches, in *Sedimentation in Volcanic Settings, SEPM Spec. Pub.* *45*, edited by R. V. Fisher and G. A. Smith, SEPM (Society for Sedimentary Geology), pp. 99–106.
- Glicken, H. (1996), Rockslide-debris avalanche of May 18, 1980, Mount St. Helens Volcano, *U.S. Geol. Surv. Open File Rep.*, *96-677*, 90 pp.
- Griswold, J. P., and R. M. Iverson (2008), Mobility statistics and automated hazard mapping for debris flows and rock avalanches (ver. 1.1, April 2014), *U.S. Geol. Surv. Sci. Invest. Rep.*, *2007-5276*, 59 pp.
- Harford, C. L., M. S. Pringle, R. S. J. Sparks, and S. R. Young (2002), The volcanic evolution of Montserrat using $^{40}\text{Ar}/^{39}\text{Ar}$ geochronology, in *The Eruption of Soufrière Hills Volcano, Montserrat, From 1995 to 1999, Mem. Geol. Soc. London* *21*, edited by T. H. Druitt and B. P. Kokelaar, pp. 93–113, Geol. Soc. of London, London, U. K.
- Herd, R. A., M. Edmonds, and V. Bass (2005), Catastrophic lava dome failure at Soufrière Hills Volcano, Montserrat 12–13 July 2003, *J. Volcanol. Geotherm. Res.*, *148*, 234–252.
- Hoblitt, R., D. Miller, and J. Vallance (1981), Origin and stratigraphy of the deposit produced by the May 18 directed blast, in *The 1980 Eruptions of Mount St. Helens, Washington, U.S. Geol. Surv. Prof. Pap.* *1250*, edited by P. Lipman and D. Mulineaux, pp. 401–419, U.S. Government Print. Off., Washington, D. C.
- Hodkinson, R. A., and D. S. Cronan (1991), Regional and depth variability in the composition of cobalt-rich ferromanganese crusts from the SOPAC area and adjacent parts of the central equatorial Pacific, *Mar. Geol.*, *98*, 437–447.
- Hunt, J. E., R. B. Wynn, D. G. Masson, P. J. Talling, and D. A. H. Teagle (2011), Sedimentological and geochemical evidence for multistage failure of volcanic island landslides: A case study from Icod landslide on north Tenerife, Canary Islands, *Geochem. Geophys. Geosyst.*, *12*, Q12007, doi:10.1029/2011GC003740.
- Iverson, R. M., et al. (2015), Landslide mobility and hazards: Implications of the 2014 Oso disaster, *Earth Planet. Sci. Lett.*, *412*, 197–208.
- John, D. A., T. W. Sisson, G. N. Breit, R. O. Rye, and J. W. Vallance (2008), Characteristics, extent and origin of hydrothermal alteration at Mount Rainier Volcano, Cascades Arc, USA: Implications for debris-flow hazards and mineral deposits, *J. Volcanol. Geotherm. Res.*, *175*, 289–314.
- Karstens, J., G. J. Crutchley, C. Berndt, P. J. Talling, S. F. L. Watt, J. Trofimovs, V. Hühnerbach, A. Le Friant, and E. Lebas (2013), Insights into pyroclastic flow emplacement from high-resolution 3D seismic data offshore Montserrat, Lesser Antilles, *J. Volcanol. Geotherm. Res.*, *257*, 1–11.
- Lebas, E., A. Le Friant, G. Boudon, S. F. L. Watt, P. J. Talling, N. Feuillet, C. Deplus, C. Berndt, and M. Vardy (2011), Multiple widespread landslides during the long-term evolution of a volcanic island: Insights from high-resolution seismic data, Montserrat, Lesser Antilles, *Geochem. Geophys. Geosyst.*, *12*, Q05006, doi:10.1029/2010GC003451.
- Le Friant, A., C. Harford, C. Deplus, G. Boudon, R. S. J. Sparks, R. Herd, and J.-C. Komorowski (2004), Geomorphological evolution of Montserrat (West Indies): Importance of flank collapse and erosional processes, *J. Geol. Soc. London*, *161*, 147–160.
- Le Friant, A., C. Deplus, G. Boudon, J.-C. Komorowski, J. Trofimovs, R. S. J. Sparks, and P. J. Talling (2009), Submarine deposition of volcaniclastic material from the 1995–2005 eruptions of the Soufrière Hills volcano, Montserrat, *J. Geol. Soc. London*, *166*, 171–182.
- Le Friant, A., et al. (2015), Submarine record of volcanic island construction and collapse in the Lesser Antilles arc: First scientific drilling of submarine volcanic island landslides by IODP Expedition 340, *Geochem. Geophys. Geosyst.*, *16*, 420–442, doi:10.1002/2014GC005652.
- Legros, F. (2002), The mobility of long-runout landslides, *Eng. Geol.*, *63*, 301–331.
- Major, J. J., and R. M. Iverson (1999), Debris-flow deposition: Effects of pore-fluid pressure and friction concentrated at flow margins, *Geol. Soc. Am. Bull.*, *111*, 1424–1434.
- Masson, D. G., A. B. Watts, M. J. R. Gee, R. Urgeles, N. C. Mitchell, T. P. Le Bas, and M. Canals (2002), Slope failures on the flanks of the western Canary Islands, *Earth Sci. Rev.*, *57*, 1–35.
- Masson, D. G., C. B. Harbitz, R. B. Wynn, G. Pedersen, and F. Lovholt (2006), Submarine landslides: Processes, triggers and hazard prediction, *Philos. Trans. R. Soc. A*, *364*, 2009–2039.
- Moore, J. G., D. A. Clague, R. T. Holcomb, P. W. Lipman, W. R. Normark, and M. E. Torresan (1989), Prodigious submarine landslides on the Hawaiian ridge, *J. Geophys. Res.*, *94*, 17,465–17,484.
- Morgan, J. K., D. A. Clague, D. C. Borchers, A. S. Davis, and K. L. Milliken (2007), Mauna Loa's submarine western flank: Landsliding, deep volcanic spreading, and hydrothermal alteration, *Geochem. Geophys. Geosyst.*, *8*, Q05002, doi:10.1029/2006GC001420.
- Naranjo, J. A., and P. Francis (1987), High velocity debris avalanche at Lastarria volcano in the north Chilean Andes, *Bull. Volcanol.*, *49*, 509–514.
- Paguican, E. M. R., B. van Wyk de Vries, and A. Lagmay (2014), Hummocks: How they form and how they evolve in rockslide-debris avalanches, *Landslides*, *11*, 67–80.
- Reimer, P. J., et al. (2013), IntCal13 and Marine13 radiocarbon age calibration curves 0–50,000 years cal BP, *Radiocarbon*, *55*, 1869–1887.

- Roobol M. J., and A. L. Smith (1998), Pyroclastic stratigraphy of the Soufrière Hills volcano, Montserrat; implications for the present eruption, *Geophys. Res. Lett.*, **25**, 3393–3396.
- Satake, K. (2007), Volcanic origin of the 1741 Oshima-Oshima tsunami in the Japan Sea, *Earth Planets Space*, **59**, 381–390.
- Shea, T., B. van Wyk de Vries, and M. Pilato (2008), Emplacement mechanisms of contrasting debris avalanches at Volcán Mombacho (Nicaragua), provided by structural and facies analysis, *Bull. Volcanol.*, **70**, 899–921.
- Siebe, C., J. C. Komorowski, and M. F. Sheridan (1992), Morphology and emplacement of an unusual debris-avalanche deposit at Jocotitlán volcano, Central Mexico, *Bull. Volcanol.*, **54**, 573–589.
- Siebert, L. (1984), Large volcanic debris avalanches: Characteristics of source areas, deposits, and associated eruptions, *J. Volcanol. Geotherm. Res.*, **22**, 163–197.
- Silver, E., S. Day, S. Ward, G. Hoffmann, P. Llanes, N. Driscoll, B. Appelgate, and S. Saunders (2009), Volcano collapse and tsunami generation in the Bismarck Volcanic Arc, Papua New Guinea, *J. Volcanol. Geotherm. Res.*, **186**, 210–222.
- Smith, A. L., M. J. Roobol, J. H. Schellekens, and G. S. Mattioli (2007), Prehistoric stratigraphy of the Soufrière Hills-South Soufrière Hills volcanic complex, Montserrat, West Indies, *J. Geol.*, **115**, 115–127.
- Stinton, A. J., P. D. Cole, H. M. Odber, T. Christopher, G. Avard, and M. Bernstein (2014), Dome growth and valley fill during Phase 5 (8 October 2009–11 February 2010) at the Soufrière Hills Volcano, Montserrat, in *The Eruption of Soufrière Hills Volcano, Montserrat, From 2000 to 2010*, *Mem. Geol. Soc. London* **39**, edited by G. Wadge, R. E. A. Robertson, and B. Voight, Geol. Soc. of London, London, U. K.
- Talling, P. J., D. G. Masson, E. J. Sumner, and G. Malgesini (2012), Subaqueous sediment density flows: Depositional processes and deposit types, *Sedimentology*, **59**, 1939–2003.
- Trofimovs, J., R. S. J. Sparks, and P. J. Talling (2008), Anatomy of a submarine pyroclastic flow and associated turbidity current: July 2003 dome collapse event, Soufrière Hills volcano, Montserrat, West Indies, *Sedimentology*, **55**, 617–634.
- Trofimovs, J., et al. (2010), Evidence for carbonate platform failure during rapid sea-level rise; ca 14000 year old bioclastic flow deposits in the Lesser Antilles, *Sedimentology*, **57**, 735–759.
- Trofimovs, J., et al. (2013), Timing, origin, and emplacement dynamics of mass flows offshore SE Montserrat in the last 110 ka: Implications for landslide and tsunami hazards, eruption history, and volcanic island evolution, *Geochem. Geophys. Geosyst.*, **14**, 385–406, doi: 10.1002/ggge.20052.
- Wadge, G., P. W. Francis, and C. F. Ramirez (1995), The Socompa collapse and avalanche event, *J. Volcanol. Geotherm. Res.*, **66**, 309–336.
- Wadge, G., B. Voight, R. S. J. Sparks, P. Cole, and S. C. Loughlin (2014), An overview of the eruption of Soufrière Hills volcano from 2000–2010, in *The Eruption of the Soufrière Hills Volcano, Montserrat from 2000–2010*, *Mem. Geol. Soc. London* **3**, edited by G. Wadge, R. E. A. Robertson, and B. Voight, pp. 1–40, Geol. Soc. of London, London, U. K.
- Wall-Palmer, D., et al. (2014), Late Pleistocene stratigraphy of IODP Site U1396 and compiled chronology offshore of south and south west Montserrat, Lesser Antilles, *Geochem. Geophys. Geosyst.*, **15**, 3000–3020, doi:10.1002/2014GC005402.
- Ward, S. N., and S. Day (2003), Ritter Island Volcano—Lateral collapse and the tsunami of 1888, *Geophys. J. Int.*, **154**, 891–902.
- Watt, S. F. L., et al. (2012a), Combinations of volcanic-flank and seafloor-sediment failure offshore Montserrat, and their implications for tsunami generation, *Earth Planet. Sci. Lett.*, **319**, 228–240.
- Watt, S. F. L., et al. (2012b), Widespread and progressive seafloor-sediment failure following volcanic debris-avalanche emplacement: Landslide dynamics and timing offshore Montserrat, Lesser Antilles, *Mar. Geol.*, **323–325**, 69–94.
- Watt, S. F. L., P. J. Talling, and J. E. Hunt (2014), New insights into the emplacement dynamics of volcanic-island landslides, *Oceanography*, **27**, 46–57.
- Yokose, H. (2002), Landslides on the Windward Flanks of Oahu and Molokai, Hawaii: SHINKAI 6500 Submersible Investigations, in *Hawaiian Volcanoes: Deep Underwater Perspectives*, vol. 128, edited E. Takahashi et al., AGU, pp. 245–261, Washington, D. C., doi:10.1029/GM128p0245.
- Yokose, H., and P. W. Lipman (2004), Emplacement mechanisms of the South Kona slide complex, Hawaii Island: Sampling and observations by remotely operated vehicle Kaiko, *Bull. Volcanol.*, **66**, 569–584.
- Zellmer, G. F., C. J. Hawkesworth, R. S. J. Sparks, L. E. Thomas, C. L. Harford, T. S. Brewer, and S. C. Loughlin (2003), Geochemical evolution of the Soufrière Hills Volcano, Montserrat, Lesser Antilles volcanic arc, *J. Petrol.*, **44**, 1349–1374.